Mechanics of Advanced Materials and Structures
Publication details, including instructions for authors and subscription information:
http://www.tandfonline.com/loi/umcm20

Computational Investigation of Glare with Several Cracks and Delaminations under Monotonic and Cyclic Loads of Constant Amplitude

Sunil Bhat[a] & Rajasekhar Patibandla[a]
[a] School of Mechanical and Building Sciences, Vellore Institute of Technology, Vellore, Tamil Nadu, India
Accepted author version posted online: 20 Aug 2012.Published online: 29 Apr 2014.

To cite this article: Sunil Bhat & Rajasekhar Patibandla (2014) Computational Investigation of Glare with Several Cracks and Delaminations under Monotonic and Cyclic Loads of Constant Amplitude, Mechanics of Advanced Materials and Structures, 21:8, 607-630, DOI: 10.1080/15376494.2012.699602

To link to this article: http://dx.doi.org/10.1080/15376494.2012.699602

Mechanics of Advanced Materials and Structures (2014) **21**, 607–630

ISSN: 1537-6494 print / 1537-6532 online
DOI: 10.1080/15376494.2012.699602

Taylor & Francis
Taylor & Francis Group

Computational Investigation of Glare with Several Cracks and Delaminations under Monotonic and Cyclic Loads of Constant Amplitude

SUNIL BHAT and RAJASEKHAR PATIBANDLA

School of Mechanical and Building Sciences, Vellore Institute of Technology, Vellore, Tamil Nadu, India

Received 26 June 2011; accepted 2 December 2011.

A residually stressed aluminum fiber metal laminate (Glare) with delaminations, caused by co-existence of normal cracks in aluminum layers and transverse interfacial cracks between aluminum and fiber layers, is theoretically and numerically investigated under monotonic and cyclic loads of constant amplitude. Double and multiple delaminations, governed by various types of debonding curves, are modeled with the help of cohesive elements. Role of fibers in load or fiber bridging over the cracks leading to enhanced fracture and fatigue properties of the laminate is demonstrated and validated. Magnitude of shielding effect at normal crack tip is quantified by stress intensity parameter and J integral values. Influence of delamination growth parameters on fiber bridging and stress state in aluminum layers is also examined. Theoretical and numerical results support each other well.

Keywords: cohesive element, delamination, fatigue, Glare, J integral, residual stress

Nomenclature

b	= delamination height at laminate edge
c	= crack length
c'	= starter notch length
$c0$	= composite layer (resin impregnated fiber) with fiber in y direction
$c90$	= composite layer with fiber in x direction
C1, C2, and C3	= cohesive element data
ds	= incremental path length
E	= modulus of elasticity
E_{lc}	= longitudinal modulus of elasticity of composite (along fiber)
E_{tc}	= transverse modulus of elasticity of composite (perpendicular to fiber)
E_{ll}	= longitudinal modulus of elasticity of laminate (y direction)
E_{tl}	= transverse modulus of elasticity of laminate (x direction)
G	= energy release rate at delamination tip
J	= J integral
K	= stress intensity parameter
m', m''	= Ramberg-Osgood constants
n	= number of layers
P	= path length
t	= thickness of layer
T	= traction
T'	= temperature
u^*	= load line crack opening displacement
u_n	= nodal displacement in x direction
v_n	= nodal displacement in y direction
v	= volume fraction of component in composite layer
v'	= volume fraction of component in laminate
V	= volume of material
w	= width of laminate
W_e	= strain energy density
Y	= yield strength
μ	= shear modulus
ν	= Poisson's ratio
δ_c	= Prepreg. deformation
δ_{ad}	= shear/adhesive deformation
δ_{al}	= deformation in aluminum
ν_{majc}	= major Poisson's ratio of composite (along the fiber w.r.t. perpendicular to fiber)
$\nu_{\min c}$	= minor Poisson's ratio of composite (perpendicular to fiber w.r.t. along the fiber)
ν_{majl}	= major Poisson's ratio of laminate (y direction w.r.t. x direction)
α	= coefficient of thermal expansion

Address correspondence to Sunil Bhat, School of Mechanical and Building Sciences, Vellore Institute of Technology, Katpadi Road, Vellore, Tamil Nadu, 632014, India. E-mail: sbhat_789@rediffmail.com

Color versions of one or more of the figures in the article can be found online at www.tandfonline.com/umcm.

α_{lc} = longitudinal coefficient of thermal expansion of composite (along fiber)
α_{tc} = transverse coefficient of thermal expansion of composite (perpendicular to fiber)
α_{ll} = longitudinal coefficient of thermal expansion of laminate (y direction)
α_{tl} = transverse coefficient of thermal expansion of laminate (x and z directions)
$\{M\}$ = stiffness matrix
σ = normal stress
τ = shear stress
ε = normal strain
γ = shear strain
Δ = parameter under cyclic load
Π = average of total stresses in all layers

Subscripts

al = an aluminum layer
ambient = ambient temperature
applied = applied value
av = average value
br = effect due to load bridging in delaminated zone
crack = effect due to crack
curing = curing temperature
*c*0 = composite *c*0
*c*90 = composite *c*90
f = a fiber layer
i, *j* = summation constants
induced = induced value
lam = laminate
r = a resin layer
rs = residual strain
tip = crack tip
total = total value in delaminated zone
*total** = total value in entire layer
x, *y*, *z* = co-ordinate system
1, 2, 3 = *c*0, *c*90 and aluminum layers
1″ to 6″ = fiber layers in the laminate

1. Introduction

Fiber metal laminate (FML) is an advanced hybrid composite that consists of layers of thin and light metallic sheets bonded alternatively by heat and pressure in an auto-clave cycle with composite prepreg. units, each unit comprising resin impregnated fiber layers laid in the same or different orientations. One such aluminum alloy and glass fiber FML, commercially known as Glare, is reported to exhibit excellent fatigue crack growth resistance. Parent crack in the loaded laminate nucleates and propagates in weak aluminum layers, whereas stronger sandwiched fibers do not fracture and remain intact thereby resulting in load or fiber bridging over the crack. Bridging diverts load towards fibers (in form of fiber bridging stress), that diminishes stress field around the crack, or shields the crack tip thereby reducing crack tip stress intensity parameter and fatigue crack growth rate. At the same time, transverse or interfacial crack can develop between aluminum and fiber layers due to the presence of cyclic shear stresses at the interfaces. Interfacial crack along with the parent crack constitute a delamination, the size of which influences the bridging stress. Delaminations of different shapes can develop in the laminate. The contour of delamination edge or debonding curve between aluminum and fiber is decided by the difference in growth rates of parent and interfacial cracks that, in turn, depends upon the material properties, strength of the adhesive bond between aluminum and fiber layers, and applied load parameters. Also, several cracks can exist in the laminate at a time leading to multiple delaminations.

Hitherto, several fatigue and fracture studies of theoretical and numerical types have been reported on FMLs under constant amplitude load in an ambient environment. Lin et al. [1] discussed the fatigue behavior in Care (carbon and aluminum based FML) followed by Lin and Kao investigating the effect of fiber bridging [2] and delamination growth [3] on crack propagation in similar laminates. Guo and Wu [4–6] presented theoretical and phenomenological models for predicting fatigue crack growths and bridging stress distribution in FML. Brown and Young [7] investigated crack and delamination growth in Arall (Kevlar and aluminum-based FML) and Glare of different thickness under constant amplitude loads at different stress levels and R ratios. Wu and Guo [8] obtained the distribution of bridging stress along the crack line and identified the factors affecting the bridging stress. A test method for determining the delamination growth rates was also presented by them. Takamatsu et al. [9] used a compliance method to analyze fatigue crack growth in FML. Homan [10] found that fatigue crack initiation in FML depends upon stress cycles in metal. He also investigated the effect of residual stress in fibers and aluminum layers over the crack tip. Alderliesten and Homan [11] discussed fatigue and damage tolerance issues of Glare in aircraft structures. Suiker and Fleck [12] presented a relation between fatigue crack growth rate and remote cyclic stress with and without the delaminations. Alderliesten [13] examined propagation of fatigue cracks in aluminum layers under the effect of delaminations. He observed stress intensity parameter at the crack tip as the function of far-field opening stress and closing bridging stress in aluminum layers. Wu et al. [14] evaluated residual strength of a notched FML. Alderliesten et al. [15] determined crack opening distribution as the result of shear deformation and validated the results with finite element analysis. Plokker et al. [16] investigated crack closure aspects in FML. Alderliesten [17] reviewed phenomenological, analytical, and finite element models for fatigue crack propagation prediction in Glare. Chang and Yang [18] studied crack tip characteristics in FML with the help of theoretical and numerical models. Khan et al. [19] investigated post-stretching stress redistribution in FML. Alderliesten and Rans [20] reported concepts of fatigue threshold in FML. Abdullah et al. [21] presented a numerical program for fatigue crack growth model and validated it with experiments. Recently, Rodi et al. [22] investigated

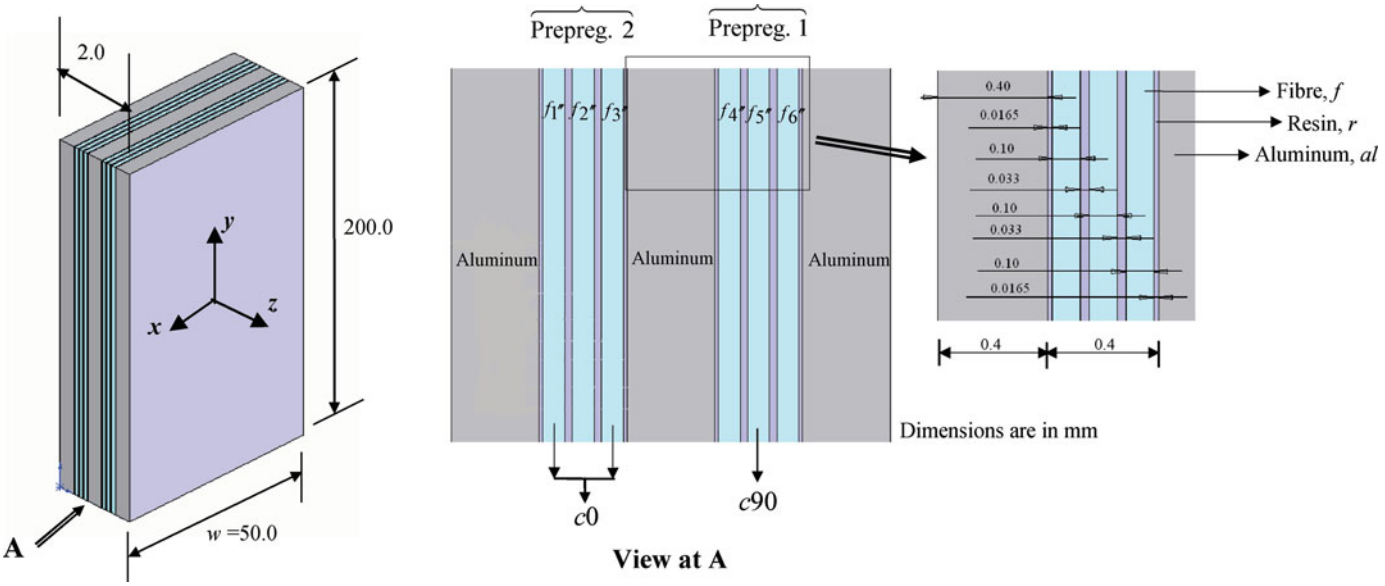

Fig. 1. Glare laminate.

applicability of crack tip opening angle (CTOA) in FML. They inferred that CTOA criterion could be successfully used for predicting the residual strength of FML.

Literature survey supports the need for a detailed study of the effect of the number and shape of delaminations over fatigue and fracture characteristics of a FML. The scope to numerically validate the theoretical model developed for determining bridging stresses in such a case also exists. The aim of this article, therefore, is to numerically model a cracked FML (Glare), with double and multiple delaminations of various shapes (triangular, cosine, parabolic and elliptical type debonding curves assumed for the purpose of computation) to assess the following in the laminate subjected to constant amplitude monotonic and cyclic load in ambient environment: (i) Change in stress fields in fibers and aluminum layers due to fiber bridging; (ii) Magnitude of bridging and its effect over normal crack tip; and (iii) Stress intensity parameter at normal crack tip post bridging. Influence of delamination growth parameters on fiber bridging and stress state in aluminum layers is also examined. The numerical results are finally compared with the theoretical ones. Since residual stresses of different magnitudes develop in the constituent materials during laminate curing due to their varying stiffness and coefficients of thermal expansion, these stresses play an important role in the mechanics of a FML and are included in the investigation.

2. Characterisation of Glare

Refer to Figure 1. Glare is assumed to comprise three 0.4-mm thick 2024-T3 aerospace aluminum alloy sheets bonded and cured alternatively with two pre-pregs., with each pre-preg. built up of three composite layers in the sequence, *c*0-*c*90-*c*0. A composite layer consists of 4 mil or 0.1-mm thick unidirectional E-glass fiber coated with epoxy resin. Composite *c*0 has fibers laid in *y* direction, i.e., along the direction of the load, whereas composite *c*90 has fibers laid in *x* direction, i.e., perpendicular to the direction of load. The laminate is 200 mm long, 50 mm wide, and 2 mm thick. Material properties [23] are presented in Table 1. Fundamental equations governing the properties of composite layers and of the overall laminate are available in Appendix A. Pertinent laminate data are provided in Table 2.

Refer to Figure 2. Two types of laminates, cured at 90 deg. and 120 deg. temperatures, are investigated under constant

Table 1. Material properties

Property	Al. 2024-T3, *al* (isotropic)	E-Glass, *f* (isotropic)	Epoxy resin, *r* (isotropic)
(i) Mod. of elasticity (E), MPa	72,000.0	71,000.0	3500.0
(ii) Shear modulus (μ), MPa	27,060.0	29,710.0	1250.0
(iii) Poisson's ratio (ν)	0.33	0.22	0.33
(iv) Yield strength (Y), MPa	345.0	—	—
(v) Ultimate tensile strength, MPa	485.0	3450.0	60.0
(vi) Percent elongation at break	18.0 (4.7 at 420 MPa)	4.8	4.0
(vii) Coeff. of thermal expansion (α), C^{-1}	23×10^{-6}	5.0×10^{-6}	57.5×10^{-6}
(viii) Plane strain fracture toughness (MPa$\sqrt{\text{m}}$)	40.0–50.0	4.0–5.0	0.5–0.7

Table 2. Laminate data

$v_f = 0.751$; $v_r = 0.249$; $v'_{al} = 0.6$; $v'_{c0} = 0.266$; $v'_{c90} = 0.134$; $E_{lc} = 54190$MPa;
$E_{tc} = 12200$MPa; $\mu_{c0} = \mu_{c90} = 4450$MPa; $E_{ll} = 59240$MPa; $E_{tl} = 41278$MPa;
$\nu_{majc} = 0.2473$; $\nu_{\min c} = 0.054$; $\nu_{majl} = 0.28$; $\alpha_{lc} = 4.69 \times 10^{-6}$; $\alpha_{tc} = 22.3 \times 10^{-6}$;
$\alpha_{ll} = 18.62 \times 10^{-6}$; $\alpha_{tl} = 17.25 \times 10^{-6}$.

far field monotonic tensile stress, $\sigma_{y,applied}$, of 150 MPa and tension–tension fatigue cycles with maximum and minimum stress values of 150 MPa and 15 MPa, respectively. Classical theory is employed to obtain stress distribution in various layers of the loaded laminate. Effect of curing is incorporated by superimposing residual curing strain with the applied strain. Refer to Appendix B for stress-strain constitutive equations in plane stress conditions—Part A for equations in aluminum and pre-pregs. and Part B for equations in aluminum, fiber, and resin layers separately. Induced stress values, $\sigma_{induced}$, in various layers, without and with the effect of residual stresses in un-cracked laminate, are available in Table 3. Through Mode I, normal edge cracks in aluminum layers and different types of delaminations are considered for fatigue and fracture analysis. Two aluminum layers are cracked in the case of double delamination (first external layer is full cracked and middle layer is half cracked), whereas all three layers are cracked in the case of multiple delaminations. Thin external resin layers of pre-pregs. are also assumed to be cracked along with aluminum layers.

3. Theoretical Treatment

3.1. *Review of Damage Mechanism*

Crack under cyclic load originates and grows in the soft aluminum layer of the laminate. In comparison with the crack in the monolithic aluminum panel, nucleation of the crack in the

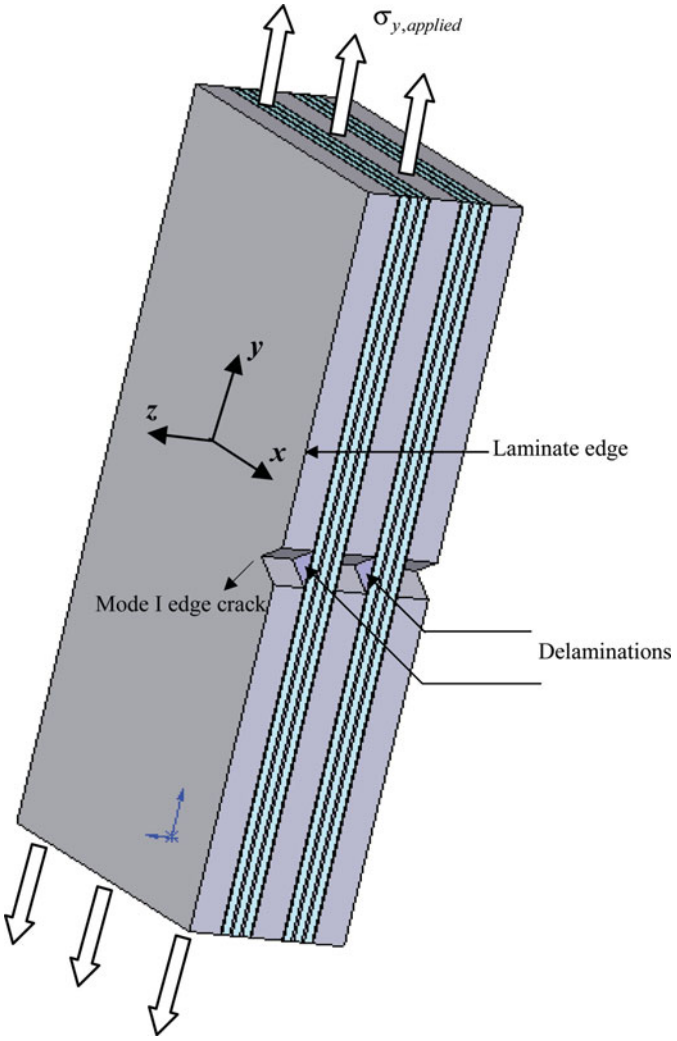

Fig. 2. Cracked and delaminated Glare.

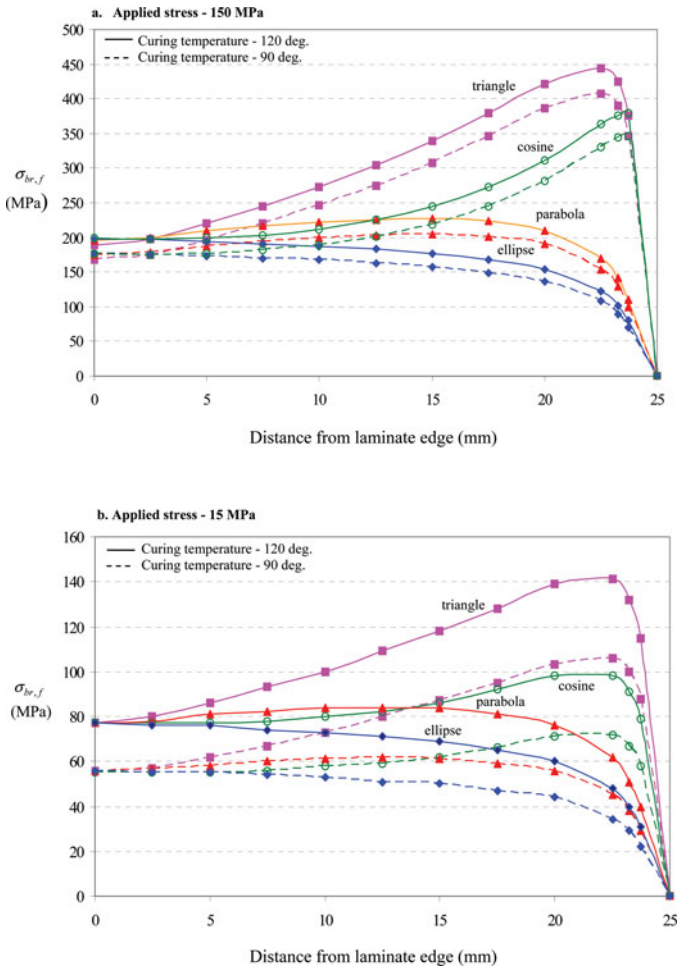

Fig. 3. Theoretical fiber bridging stresses, $\sigma_{br,f}$, for different delamination shapes, in delaminated fiber zone of laminate with double delamination.

Table 3. Stress-strain values

(A) Aluminum and Pre-preg.

$$\{M\}_{al} = \begin{bmatrix} 80.79 & 26.66 & 0 \\ 26.66 & 80.79 & 0 \\ 0 & 0 & 27.06 \end{bmatrix} \text{GPa}; \quad \{M\}_{c0} = \begin{bmatrix} 12.37 & 3.05 & 0 \\ 2.96 & 54.95 & 0 \\ 0 & 0 & 4.45 \end{bmatrix} \text{GPa}; \quad \{M\}_{c90} = \begin{bmatrix} 54.95 & 2.96 & 0 \\ 3.05 & 12.37 & 0 \\ 0 & 0 & 4.45 \end{bmatrix} \text{GPa};$$

$$\{M\}_{lam} = \begin{bmatrix} 59.06 & 17.20 & 0 \\ 17.18 & 64.725 & 0 \\ 0 & 0 & 18.01 \end{bmatrix} \text{GPa}; \quad \{M\}^{-1}_{lam} = \begin{bmatrix} 0.018 & -0.00482 & 0 \\ -0.0048 & 0.0166 & 0 \\ 0 & 0 & 0.055 \end{bmatrix}.$$

$$\text{For } \sigma_{applied} = \begin{Bmatrix} 0 \\ 150 \\ 0 \end{Bmatrix} \text{MPa}; \quad \varepsilon_{lam} = \begin{Bmatrix} -0.723 \times 10^{-3} \\ 2.49 \times 10^{-3} \\ 0 \end{Bmatrix}.$$

$$\text{For } \sigma_{applied} = \begin{Bmatrix} 0 \\ 15 \\ 0 \end{Bmatrix} \text{MPa}; \quad \varepsilon_{lam} = \begin{Bmatrix} -0.0723 \times 10^{-3} \\ 0.249 \times 10^{-3} \\ 0 \end{Bmatrix}.$$

Induced stresses, $\begin{Bmatrix} \sigma_x \\ \sigma_y \\ \tau_{xy} \end{Bmatrix}_{induced}$, for $T_{ambient} = 30\,\text{deg.}$, $T_{curing} = 90\,\text{deg.}, 120\,\text{deg.}$ are given as under:

$$\{\sigma\}_{induced,al} = \left[\begin{matrix} \text{Applied stress: 150 MPa} \\ \text{w/o rs} \quad \text{90 deg.} \quad \text{120 deg.} \end{matrix} \quad \begin{Bmatrix} 7.98 \\ 181.89 \\ 0 \end{Bmatrix} \begin{Bmatrix} 42.77 \\ 212.09 \\ 0 \end{Bmatrix} \begin{Bmatrix} 60.13 \\ 227.18 \\ 0 \end{Bmatrix} \quad \begin{matrix} \text{Applied stress: 15 MPa} \\ \text{w/o rs} \quad \text{90 deg.} \quad \text{120 deg.} \end{matrix} \quad \begin{Bmatrix} 0.798 \\ 18.19 \\ 0 \end{Bmatrix} \begin{Bmatrix} 35.59 \\ 48.53 \\ 0 \end{Bmatrix} \begin{Bmatrix} 53.01 \\ 63.78 \\ 0 \end{Bmatrix} \right] \text{MPa}.$$

Residual stresses at 90 deg. curing = 34.79 MPa (+ve) in x dir., 30.34 MPa (+ve) in y dir.
Residual stresses at 120 deg. curing = 52.15 MPa (+ve, tensile) in x dir., 45.29 MPa (+ve) in y dir.

$$\{\sigma\}_{induced,c0} = \left[\begin{matrix} \text{w/o rs} \quad \text{90 deg.} \quad \text{120 deg.} \end{matrix} \quad \begin{Bmatrix} -1.34 \\ 134.68 \\ 0 \end{Bmatrix} \begin{Bmatrix} -0.162 \\ 89.40 \\ 0 \end{Bmatrix} \begin{Bmatrix} 0.45 \\ 67.34 \\ 0 \end{Bmatrix} \quad \begin{matrix} \text{w/o rs} \quad \text{90 deg.} \quad \text{120 deg.} \end{matrix} \quad \begin{Bmatrix} -0.134 \\ 13.46 \\ 0 \end{Bmatrix} \begin{Bmatrix} 1.05 \\ -31.51 \\ 0 \end{Bmatrix} \begin{Bmatrix} 1.67 \\ -53.82 \\ 0 \end{Bmatrix} \right] \text{MPa}.$$

Residual stresses at 90 deg. curing = 1.178 MPa (+ve) in x dir., 45.29 MPa (-ve) in y dir.
Residual stresses at 120 deg. curing = 1.79 MPa (+ve) in x dir., 67.34 MPa (-ve, compressive) in y dir.

$$\{\sigma\}_{induced,c90} = \left[\begin{matrix} \text{w/o rs} \quad \text{90 deg.} \quad \text{120 deg.} \end{matrix} \quad \begin{Bmatrix} -32.35 \\ 28.59 \\ 0 \end{Bmatrix} \begin{Bmatrix} -72.75 \\ 29.03 \\ 0 \end{Bmatrix} \begin{Bmatrix} -93.30 \\ 29.25 \\ 0 \end{Bmatrix} \quad \begin{matrix} \text{w/o rs} \quad \text{90 deg.} \quad \text{120 deg.} \end{matrix} \quad \begin{Bmatrix} -3.235 \\ 2.859 \\ 0 \end{Bmatrix} \begin{Bmatrix} -43.67 \\ 3.30 \\ 0 \end{Bmatrix} \begin{Bmatrix} -64.22 \\ 3.51 \\ 0 \end{Bmatrix} \right] \text{MPa}.$$

Residual stresses at 90 deg. curing = 40.4 MPa (-ve) in x dir., 0.44 MPa (+ve) in y dir.
Residual stresses at 120 deg. curing = 60.95 MPa (-ve) in x dir., 0.66 MPa (+ve) in y dir.

(B) Individual layers

$$\{M\}_{al} = \begin{bmatrix} 80.79 & 26.66 & 0 \\ 26.66 & 80.79 & 0 \\ 0 & 0 & 27.06 \end{bmatrix} \text{GPa}; \{M\}_{r} = \begin{bmatrix} 3.92 & 1.29 & 0 \\ 1.29 & 3.92 & 0 \\ 0 & 0 & 1.25 \end{bmatrix} \text{GPa}; \{M\}_{f} = \begin{bmatrix} 74.61 & 16.41 & 0 \\ 16.41 & 74.61 & 0 \\ 0 & 0 & 29.70 \end{bmatrix} \text{GPa};$$

$$\{M\}_{lam} = \begin{bmatrix} 71.22 & 21.04 & 0 \\ 21.04 & 71.22 & 0 \\ 0 & 0 & 25.26 \end{bmatrix} \text{GPa}; \{M\}^{-1}_{lam} = \begin{bmatrix} 0.0153 & -0.0045 & 0 \\ -0.0045 & 0.0153 & 0 \\ 0 & 0 & 0.0395 \end{bmatrix}.$$

$$\text{For } \sigma_{applied} = \begin{Bmatrix} 0 \\ 150 \\ 0 \end{Bmatrix} \text{MPa}; \varepsilon_{lam} = \begin{Bmatrix} -6.75 \times 10^{-4} \\ 2.29 \times 10^{-3} \\ 0 \end{Bmatrix}.$$

(Continued on next page)

Table 3. Stress-strain values *(Continued)*

For $\sigma_{applied} = \begin{Bmatrix} 0 \\ 15 \\ 0 \end{Bmatrix}$ MPa; $\varepsilon_{lam} = \begin{Bmatrix} -0.675 \times 10^{-4} \\ 0.229 \times 10^{-3} \\ 0 \end{Bmatrix}$.

Induced stresses: $\begin{Bmatrix} \sigma_x \\ \sigma_y \\ \tau_{xy} \end{Bmatrix}_{induced}$ for $T_{ambient} = 30\,\text{deg.}$, $T_{curing} = 90\,\text{deg.}, 120\,\text{deg.}$ are as follows:

$$\{\sigma\}_{induced,al} = \left[\begin{matrix} \text{Applied stress: 150 MPa} \\ \text{w/o rs} \quad \text{90 deg.} \quad \text{120 deg.} \end{matrix} \quad \begin{matrix} \text{Applied stress: 15 MPa} \\ \text{w/o rs} \quad \text{90 deg.} \quad \text{120 deg.} \end{matrix} \right.$$
$$\left. \begin{Bmatrix} 6.50 \\ 167.0 \\ 0 \end{Bmatrix} \begin{Bmatrix} 41.32 \\ 197.14 \\ 0 \end{Bmatrix} \begin{Bmatrix} 58.79 \\ 212.6 \\ 0 \end{Bmatrix} \quad \begin{Bmatrix} 0.650 \\ 16.70 \\ 0 \end{Bmatrix} \begin{Bmatrix} 35.46 \\ 47.05 \\ 0 \end{Bmatrix} \begin{Bmatrix} 52.88 \\ 62.30 \\ 0 \end{Bmatrix} \right] \text{MPa.}$$

Residual stresses at 90 deg. curing = 34.82 MPa (+ve) in x dir., 30.14 MPa (+ve) in y dir.
Residual stresses at 120 deg. curing = 52.29 MPa (+ve) in x dir., 45.6 MPa (+ve) in y dir.

$$\{\sigma\}_{induced,r} = \left[\begin{matrix} \text{w/o rs} \quad \text{90 deg.} \quad \text{120 deg.} \end{matrix} \quad \begin{matrix} \text{w/o rs} \quad \text{90 deg.} \quad \text{120 deg.} \end{matrix} \right.$$
$$\left. \begin{Bmatrix} 0.308 \\ 8.1 \\ 0 \end{Bmatrix} \begin{Bmatrix} 12.78 \\ 20.35 \\ 0 \end{Bmatrix} \begin{Bmatrix} 19.00 \\ 26.45 \\ 0 \end{Bmatrix} \quad \begin{Bmatrix} 0.0308 \\ 0.81 \\ 0 \end{Bmatrix} \begin{Bmatrix} 12.46 \\ 13.01 \\ 0 \end{Bmatrix} \begin{Bmatrix} 18.70 \\ 19.12 \\ 0 \end{Bmatrix} \right] \text{MPa.}$$

Residual stresses at 90 deg. curing = 12.47 MPa (+ve) in x dir., 12.25 MPa (+ve) in y dir.
Residual stresses at 120 deg. curing = 18.69 MPa (+ve) in x dir., 18.35 MPa (+ve) in y dir.

$$\{\sigma\}_{induced,f} = \left[\begin{matrix} \text{w/o rs} \quad \text{90 deg.} \quad \text{120 deg.} \end{matrix} \quad \begin{matrix} \text{w/o rs} \quad \text{90 deg.} \quad \text{120 deg.} \end{matrix} \right.$$
$$\left. \begin{Bmatrix} -12.78 \\ 159.78 \\ 0 \end{Bmatrix} \begin{Bmatrix} -81.0 \\ 86.53 \\ 0 \end{Bmatrix} \begin{Bmatrix} -114.87 \\ 50.7 \\ 0 \end{Bmatrix} \quad \begin{Bmatrix} -1.278 \\ 15.978 \\ 0 \end{Bmatrix} \begin{Bmatrix} -69.48 \\ -57.03 \\ 0 \end{Bmatrix} \begin{Bmatrix} -103.33 \\ -93.0 \\ 0 \end{Bmatrix} \right] \text{MPa.}$$

Residual stresses at 90 deg. curing = 68.22 MPa (-ve) in x dir., 73.25 MPa (-ve) in y dir.
Residual stresses at 120 deg. curing = 102.09 MPa (-ve) in x dir., 109.08 MPa (-ve) in y dir.

laminate is faster since $\sigma_{y,induced,al} > \sigma_{y,applied}$, but crack propagation is much slower due to the presence of fibers [24] as discussed in the succeeding section.

The originated parent normal crack in the aluminum layer is fully constrained and cannot open for growth due to the resistance offered by sandwiched intact fiber layers. Opening occurs due to development of transverse or interfacial crack at the aluminum-fiber interface by cyclic shear stresses, generated by load transfer from aluminum to fiber layer, that induce shear/adhesive deformations leading to adhesive failure. Consequently, the parent crack opening becomes nonzero that generates stress intensity at the crack tip causing crack growth. With parent crack growth, there is again fiber bridging or diversion of load over the crack towards the fibers that triggers interfacial crack growth with consequent restraining or shielding effect at the parent crack tip. With an increase in interfacial crack length, the length over which the fibers are elongated increases resulting in lower fiber stress and transfer of the load back towards the parent crack tip that drives the parent crack. As such, the growth of parent and interfacial cracks, leading to the development and expansion of delamination between the aluminum-fiber layer, forms a balanced and coupled process albeit with opposite load transfer effects. Consequently, the magnitude of stress intensity at the parent crack tip continuously fluctuates during parent and interfacial crack growths. Conventional crack growth principles under cyclic loads, i.e., ΔK at the parent crack tip and ΔG at the interfacial crack tip exceeding the respective cyclic threshold values, hold good.

Despite an increase in delamination size with growing laminate damage, the strong fiber layers in the laminate remain intact and, as a result, a significant part of the applied load continues to be transferred over the parent crack through fibers thereby restricting the stress field and the opening of the parent crack, which eventually, at all crack lengths, leads to the enhanced fatigue properties of the laminate vis-à-vis the monolithic aluminum panel with normal crack of similar sizes.

3.2. *Model for Stress Intensity Parameter at Normal Crack Tip*

The applied stress intensity parameter, $K_{applied}$, over Mode I crack of length, c, is obtained from Eq. (1) that is based upon

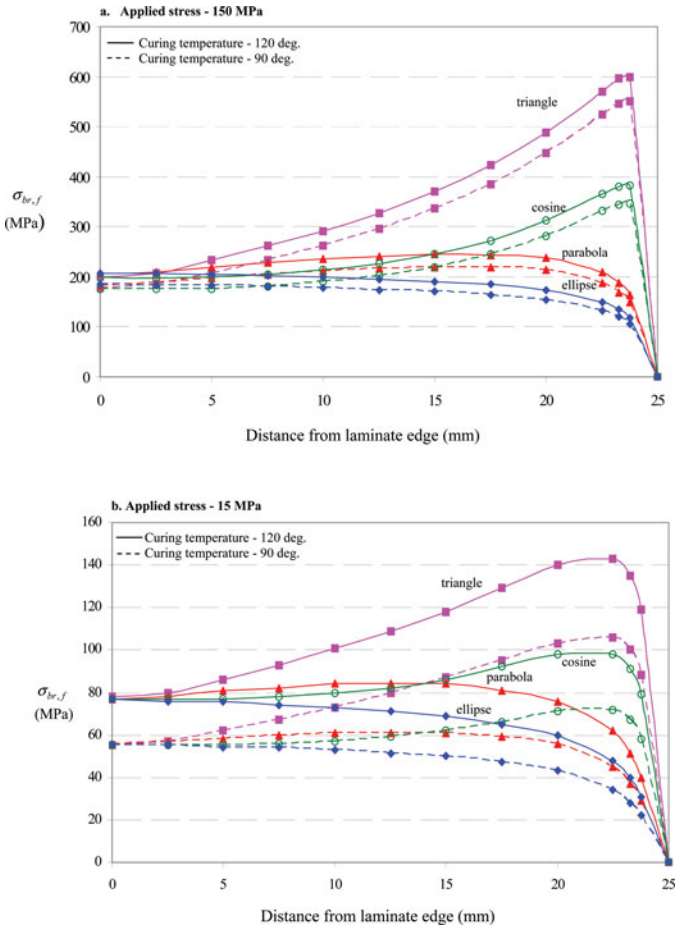

Fig. 4. Theoretical fiber bridging stresses, $\sigma_{br,f}$, for different delamination shapes, in delaminated fiber zone of laminate with multiple delaminations.

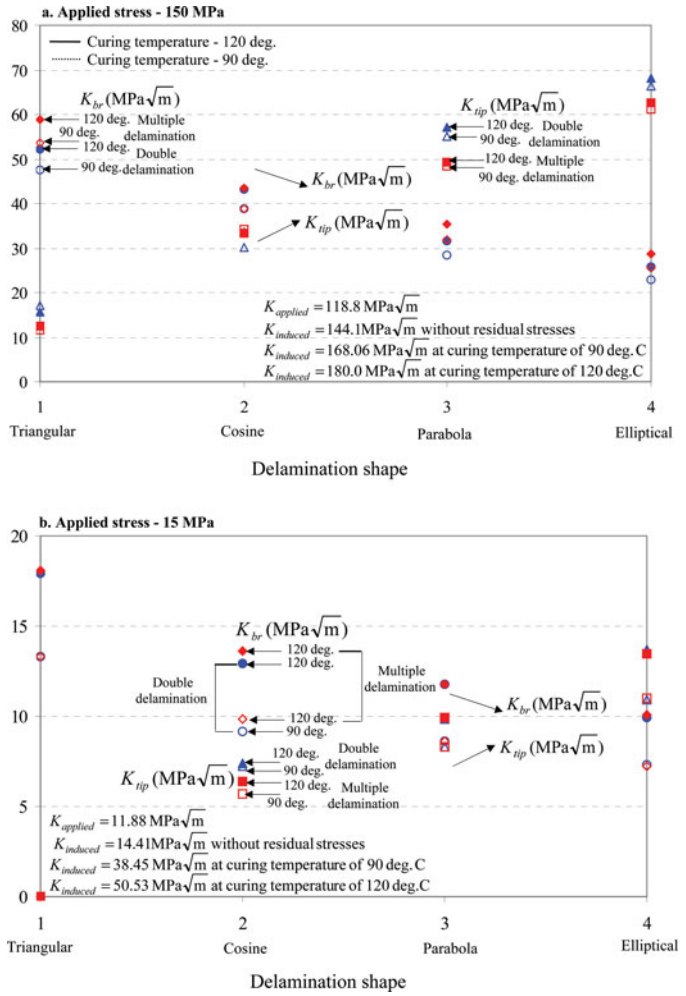

Fig. 5. Theoretical bridging and normal crack tip stress intensity parameters, K_{br} and K_{tip}, in laminates with different delaminations.

the principles of conventional linear elastic fracture mechanics (LEFM):

$$K_{applied} = \sigma_{y,induced,al} \times \sqrt{\pi c} \times CF, \tag{1}$$

where configuration factor, CF, for an edge crack [25] is empirically given by Eq. (2):

$$CF = \left[1.12 - 0.23\frac{c}{w} + 10.6\left(\frac{c}{w}\right)^2 - 21.7\left(\frac{c}{w}\right)^3 + 30.4\left(\frac{c}{w}\right)^4\right], \tag{2}$$

where w is the width of the laminate. For the delaminated zone with parent normal crack length, c, and interfacial crack height, b, at the laminate edge, the formulations [13] to determine the tensile stress transferred to fiber, $\sigma_{br,f}$, and closing compressive stress induced in aluminum, $\sigma_{br,al}$, in the delaminated zone are consolidated in Appendix C. The equations of deformation are written at several points along the crack axis in the delamination zone. Induced load line stress values

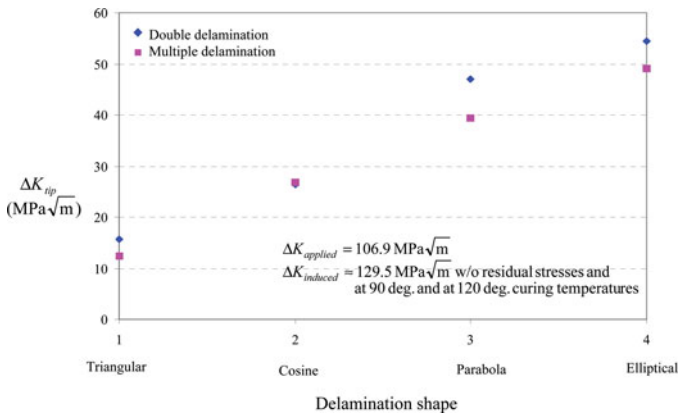

Fig. 6. Theoretical cyclic stress intensity parameter, ΔK_{tip}, in laminates with different delaminations.

Table 4. Finite element values of normal crack tip parameter

	Delamination shape							
	Triangular		Cosine		Parabolic		Elliptical	
Parameter (in aluminum layer)	A	B	A	B	A	B	A	B
Double delamination								
J_{tip} (N/mm), 150 MPa	5.4	4.58	6.14	5.17	7.66	6.52	7.93	6.70
15 MPa	0.33	0.19	0.40	0.23	0.53	0.30	0.54	0.31
K_{tip}(MPa$\sqrt{\text{m}}$), 150 Mpa	19.85	18.18	21.03	19.3	23.49	21.67	23.89	21.97
15 Mpa	4.90	3.70	5.38	4.07	6.21	4.69	6.25	4.70
ΔK_{tip}(MPa$\sqrt{\text{m}}$)	14.95	14.48	15.65	15.23	17.28	16.98	17.64	17.27
Multiple delaminations								
J_{tip} (N/mm), 150 MPa	4.94	3.73	6.61	5.64	6.70	5.74	7.25	6.18
15 MPa	0.25	0.10	0.37	0.21	0.46	0.26	0.48	0.28
K_{tip}(MPa$\sqrt{\text{m}}$), 150 Mpa	18.86	16.4	20.11	18.46	21.97	20.34	22.85	21.09
15 Mpa	4.24	2.68	5.18	3.89	4.37	4.37	5.90	4.44
ΔK_{tip}(MPa$\sqrt{\text{m}}$)	14.62	13.72	14.93	14.57	16.21	15.97	16.95	16.65

A: 120 deg. cured laminate; B: 90 deg. cured laminate.

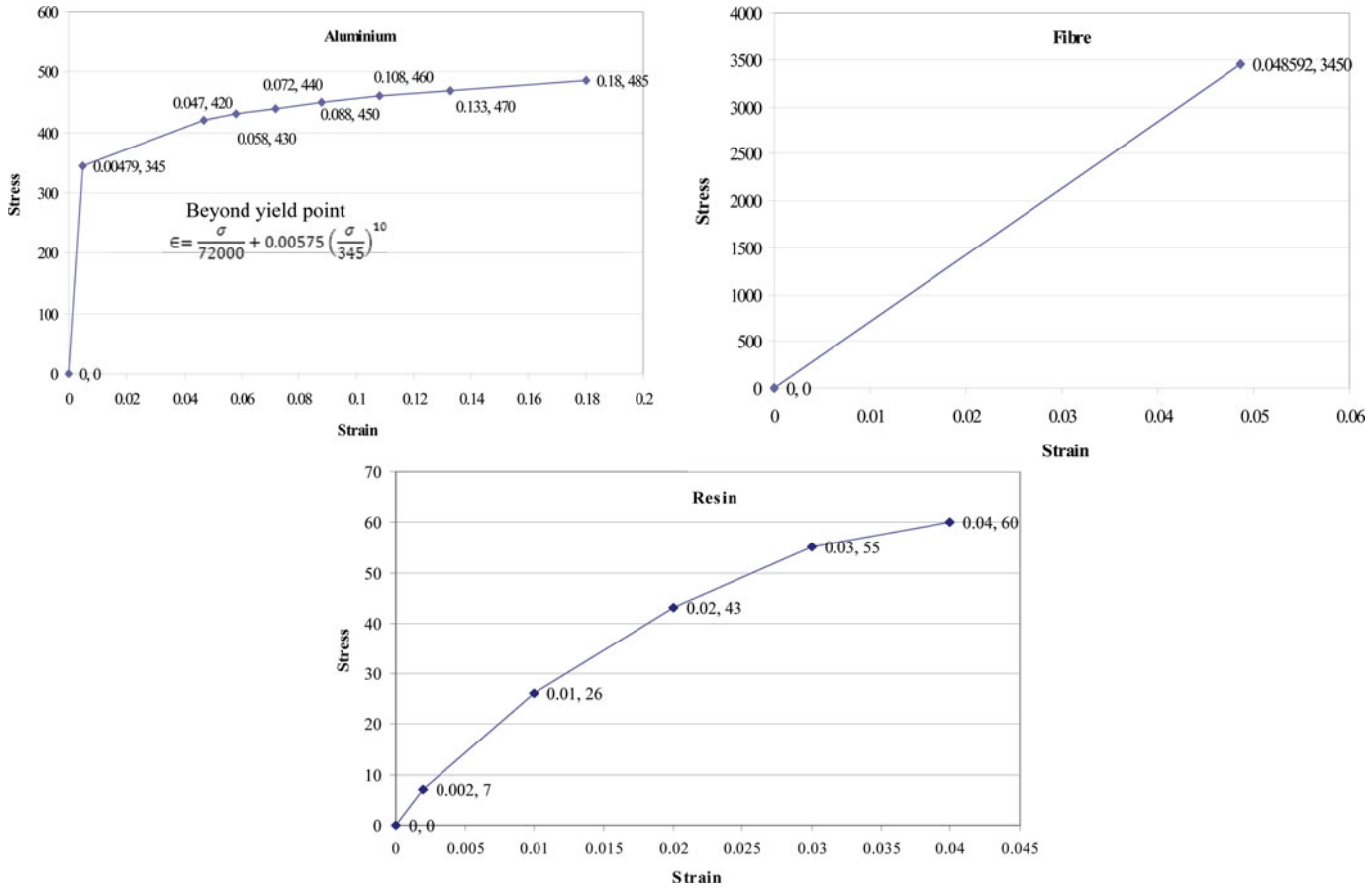

Fig. 7. Stress-strain plots of materials.

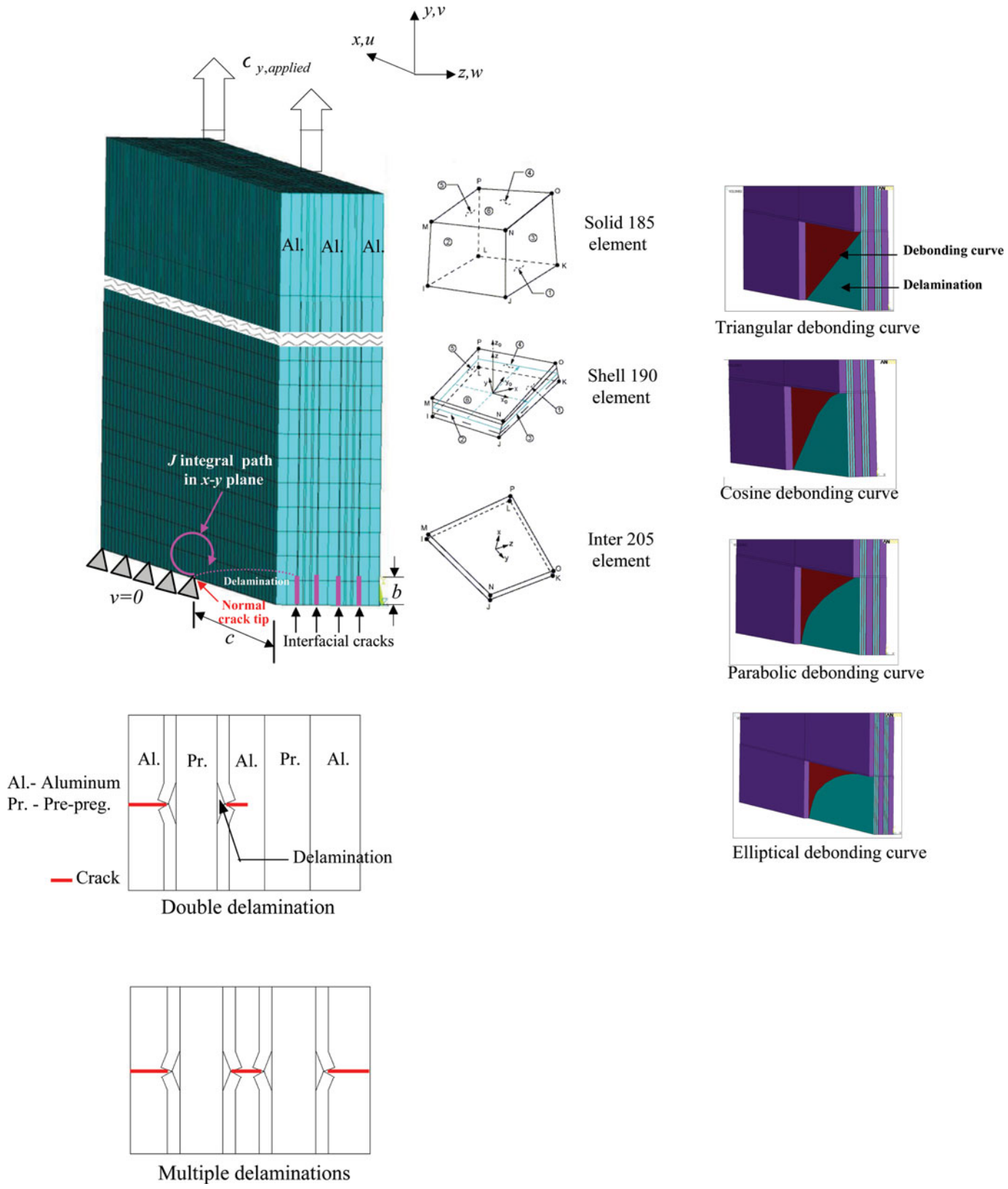

Fig. 8. Meshed model and delamination shapes.

(in y direction) in aluminum and in composite layers that are used in the formulations are picked up from Section A of Table 3. The coupled equations are solved by Jacobi's numerical iterative scheme to obtain $\sigma_{br,f}$ at the selected points while fulfilling the boundary condition of $\sigma_{br,f}$ as zero at the crack tip line. $\sigma_{br,al}$ is finally computed. Crack bridging stress intensity parameter, K_{br}, is found from Eq. (3):

$$K_{br} = 2\sum_{i=1}^{n} \frac{\sigma_{br,al}(x_i)dx}{\sqrt{\pi c}} \frac{c}{\sqrt{c^2 - x_i^2 + b_i^2}} \times \left[1 + \frac{1}{2}\left(1 + \nu_{majl}\right)\frac{b_i^2}{c^2 - x_i^2 + b_i^2}\right]. \quad (3)$$

Stress intensity parameter at normal crack tip, K_{tip}, is obtained by subtracting the bridging effects from $K_{applied}$. K_{tip} is approximated as $\frac{2}{3}K_{applied} - 2K_{br}$ in the laminate with double delamination. A factor of 2 is used to account for bridging due to two delaminations. Since there are only two cracked aluminum layers that are restrained by a third layer at the free end, $K_{applied}$ is reduced by a factor of 2/3 (2 representing the number of cracked aluminum layers and 3 the total number of aluminum layers). In the case of multiple delaminations, K_{tip} is approximated as $K_{applied} - 4K_{br}$. A factor of 4 accounts for bridging by four delaminations. As all three aluminum layers are cracked up to free ends, no reduction factor is employed in $K_{applied}$.

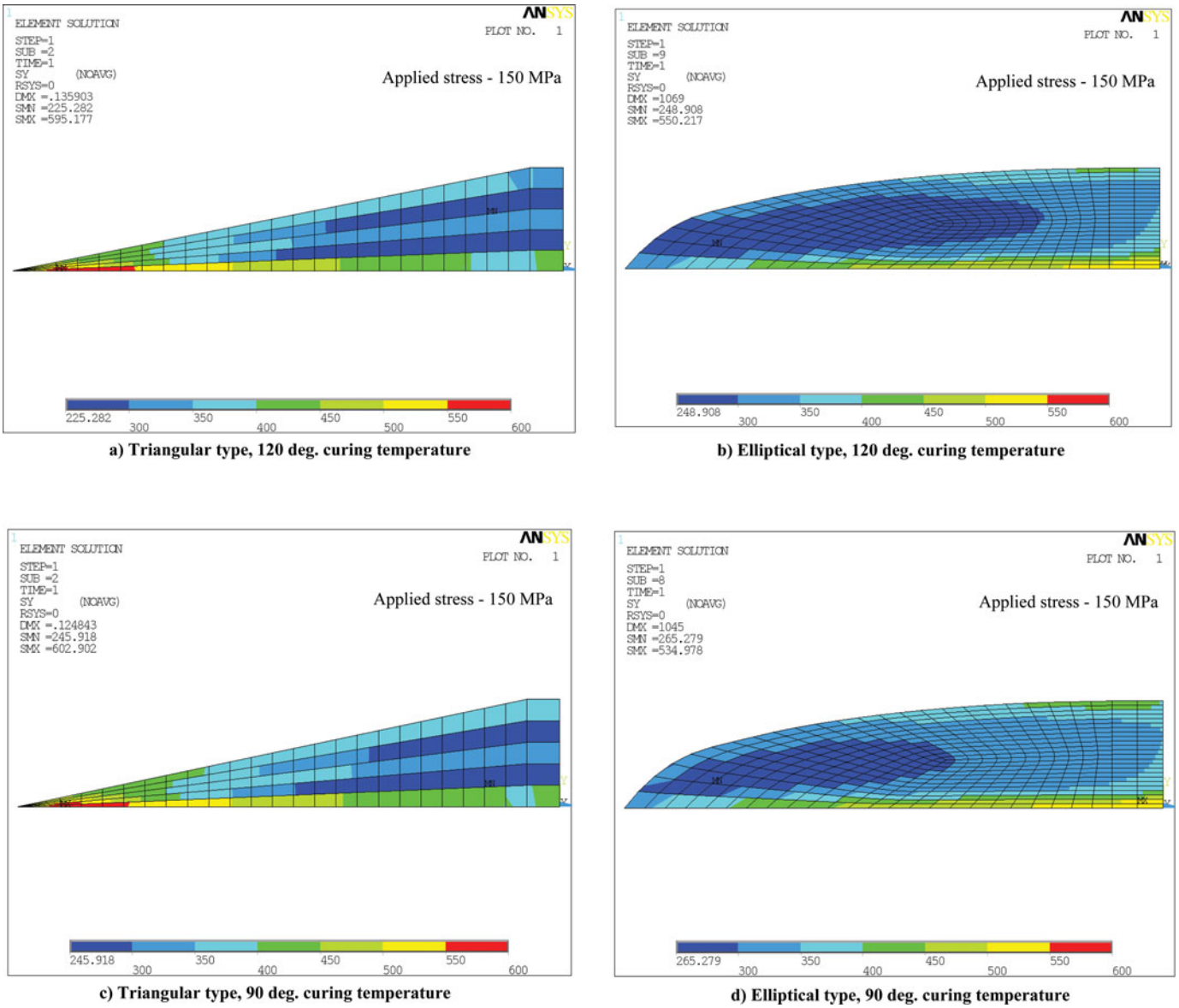

a) Triangular type, 120 deg. curing temperature

b) Elliptical type, 120 deg. curing temperature

c) Triangular type, 90 deg. curing temperature

d) Elliptical type, 90 deg. curing temperature

Fig. 9. Stress plots in y direction, $\sigma_{y,total,f}$, in delaminated fiber zone of laminate with double delamination.

3.3. *Results and Discussion*

The theoretical model is first executed over double and multiple cracked laminates with different residual stresses and delamination shapes under far-field or applied monotonic stress of 150 MPa and 15 MPa separately. The type of delamination shape decides the value of delamination height, b_i, at various x_i (refer to Appendix C). Values of t_{c0}, t_{c90}, and t_{al} are taken as 0.133, 0.133, and 0.4 mm, respectively. Data of the delaminated zone are suitably assumed, i.e., $c = 25$ mm, $b = 4.7$ mm, and $c' = 1.5$ mm [13]. Limit load of cracked aluminum layer is 3450 N. But induced load over aluminum layer of 90 deg. and 120 deg. cured laminates is 3942.8 N and 4252 N respectively, which indicates plastic collapse conditions. However, as already discussed, fiber bridging causes drop in load over aluminum layer that prevents collapse. This is also confirmed in finite element analysis as well. As such, the selected crack configuration is justified. $n_1 = 2, n_2 = 1$, and $n_3 = 2$ in the case of double delamination, whereas $n_1 = 4, n_2 = 2$, and $n_3 = 4$ in the case of multiple delaminations. $\sigma_{br,f}$ is found to be tensile (+ve), whereas $\sigma_{br,al}$ is compressive (-ve) in all the cases. Values of $\sigma_{br,f}$ at various locations along parent crack depth in delaminated fiber zones of laminates, under 150 MPa stress, with double and multiple delaminations of different shapes are provided in Figures 3 and 4, respectively. Similar trends are observed under 15 MPa stress. $\sigma_{br,f}$, in general, is least at the laminate edge, increases along the crack depth, and finally drops sharply to zero at the crack tip line. The values are maximum in the laminate with triangular delamination and least in the laminate with elliptical delamination and are more in 120 deg. cured laminate than in 90 deg. cured laminate. Crack tip shielding is confirmed by +ve values of K_{br}, which, for different delamination shapes, are plotted in Figure 5. As expected, they are maximum in the case of triangular

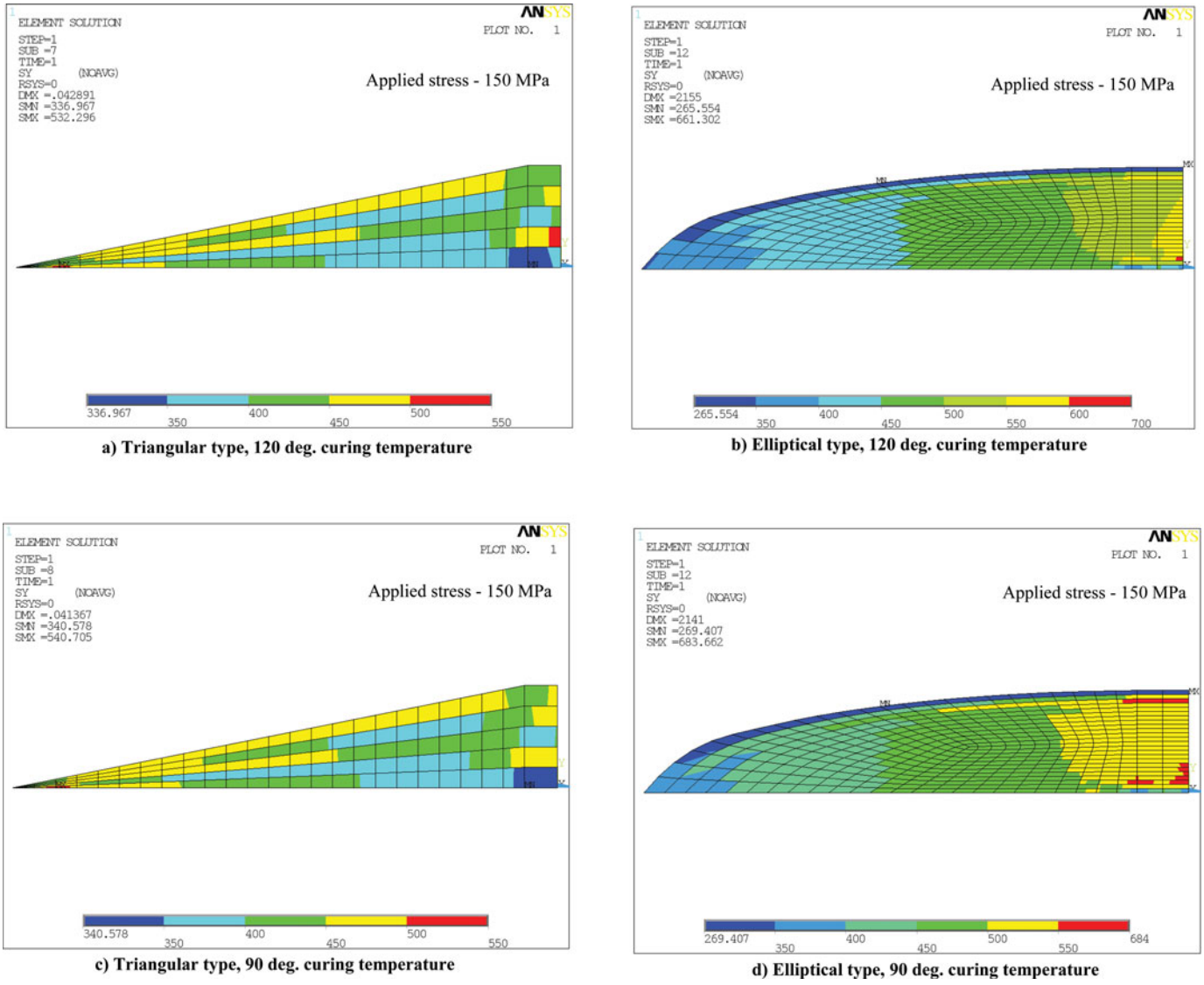

Fig. 10. Stress plots in y direction, $\sigma_{y,total,f}$, in delaminated fiber zone of laminate with multiple delaminations.

delamination and minimum in the case of elliptical delamination. Consequently, K_{tip} values are least in the former and maximum in the latter. Although fiber bridging is more in 120 deg. cured laminate than in the 90 deg. cured one, K_{tip} is found to be more in the former than in the latter. This is due to higher $\sigma_{y,induced,al}$ value in 120 deg. cured laminate that results in increased $K_{applied}$ value and, therefore, higher value of K_{tip} after subtracting the bridging effects. Bridging effects are higher in the laminates with multiple delaminations than with double delamination.

Results of monotonic load cases are subsequently used to obtain cyclic values by subtracting the results of 150 MPa and 15 MPa. Laminate curing temperature/residual stresses do not influence $\Delta K_{applied}$ values. For a particular delamination shape, ΔK_{br} and ΔK_{tip} values are nearly the same in 90 deg. and 120 deg. cured laminates and are quite close to each other in the laminates with double and multiple delaminations as well. ΔK_{tip} values are plotted in Figure 6. Like in monotonic load cases, ΔK_{tip} values are minimum in the case of triangular delamination and maximum in the case of elliptical delamination.

4. Finite Element Analysis

A 3D model of a laminate is created with 8 noded, solid 185 elements in aluminum and 8 noded, layered solid shell 190 elements in fiber and resin layers. Half of the laminate is only modeled due to symmetry. The number of nodes and elements generated are equal to 55,827 and 53,066, respectively. Linear and nonlinear stress-strain data of materials, shown in Figure 7, are used in the material models. Ramberg-Osgood equation, $\varepsilon = \frac{\sigma}{E_{al}} + \frac{Y_{al}m'}{E_{al}}(\frac{\sigma}{Y_{al}})^{m''}$ [26], is employed to obtain

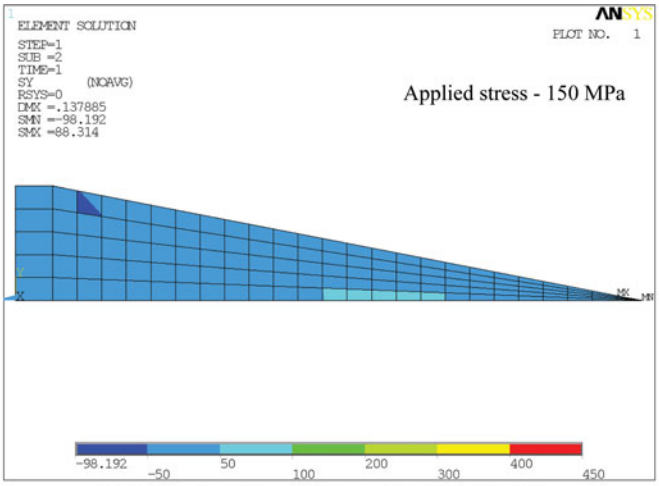

a) Triangular type, 120 deg. curing temperature

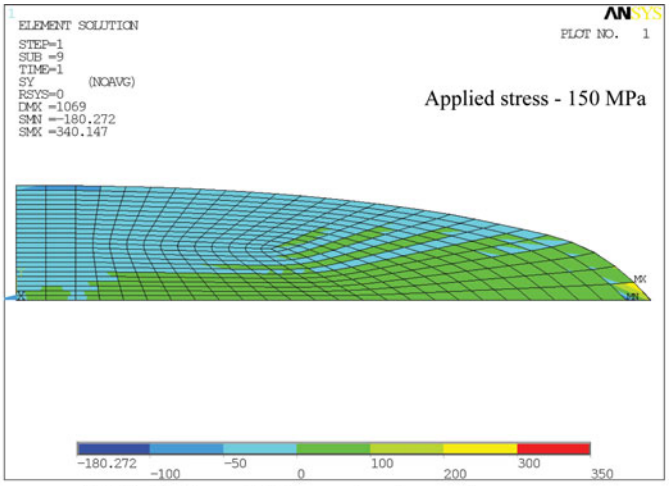

b) Elliptical type, 120 deg. curing temperature

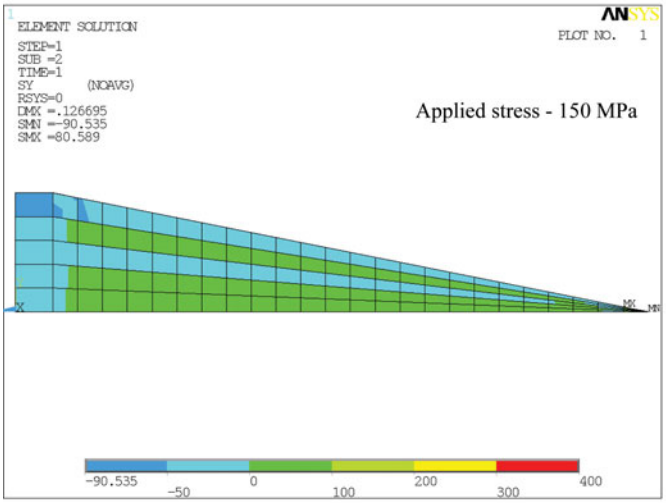

c) Triangular type, 90 deg. curing temperature

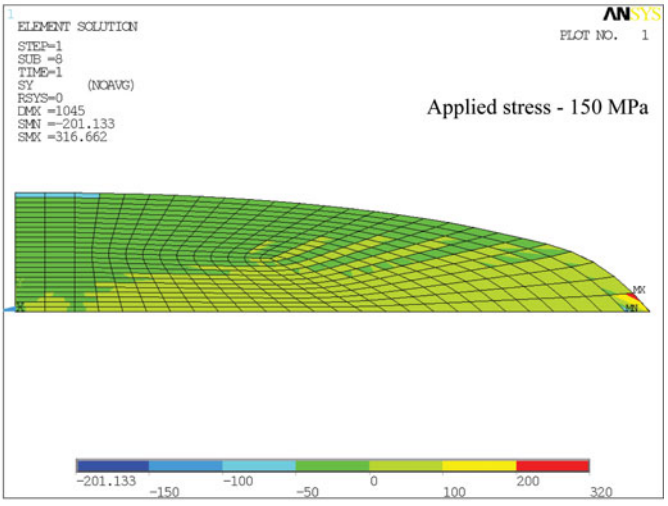

d) Elliptical type, 90 deg. curing temperature

Fig. 11. Stress plots in y direction, $\sigma_{y,total,al}$, in delaminated aluminum zone of laminate with double delamination.

nonlinear values. The material constants for aluminum, using stress-strain values at the break and at an intermediate point provided in Table 1, are obtained as $m' = 1.2$ and $m'' = 10$. The nodes representing cracks at the bottom surface in aluminum and resin layers of the model are unconstrained while all the nodes of fiber layers are constrained in y direction ($y = 0$). Load is applied as monotonic stress at the top edge of the laminate whereas the residual stresses, whose values in individual layers are taken from Section B of Table 3, are introduced over respective nodes in x and y directions. A mesh model of the laminate with various delamination shapes is shown in Figure 8. Similar models are developed with both double and multiple delaminations. Delaminations of triangular, cosine, parabolic, and elliptical debonding types (delamination dimensions already stated in Section 3.3) are modeled with the help of 8 noded, inter 205, cohesive elements. Values of maximum normal traction (σ_z), width, and maximum equivalent shear traction of τ_{zy} and τ_{zx} at the delamination zone are input as C1, C2, and C3, respectively, in the cohesive element code. Since the type of de-bonding curve influences these values, albeit marginally, the cohesive element data are found for each of them by modeling cracked laminates without delaminations but with the use of a chosen debonding curve to note the maximum values developing near the curve. Sample values of C1, C2, and C3 in the laminate, with double delamination of triangular type, cured at 120 deg. temperature are of the order of 19.5 MPa, 0.001 mm, and 15.03 MPa, respectively. All of the interface layers are glued, the common nodes are merged, and their connectivity is checked before running the models for a solution. J integral over the cyclic path, P,

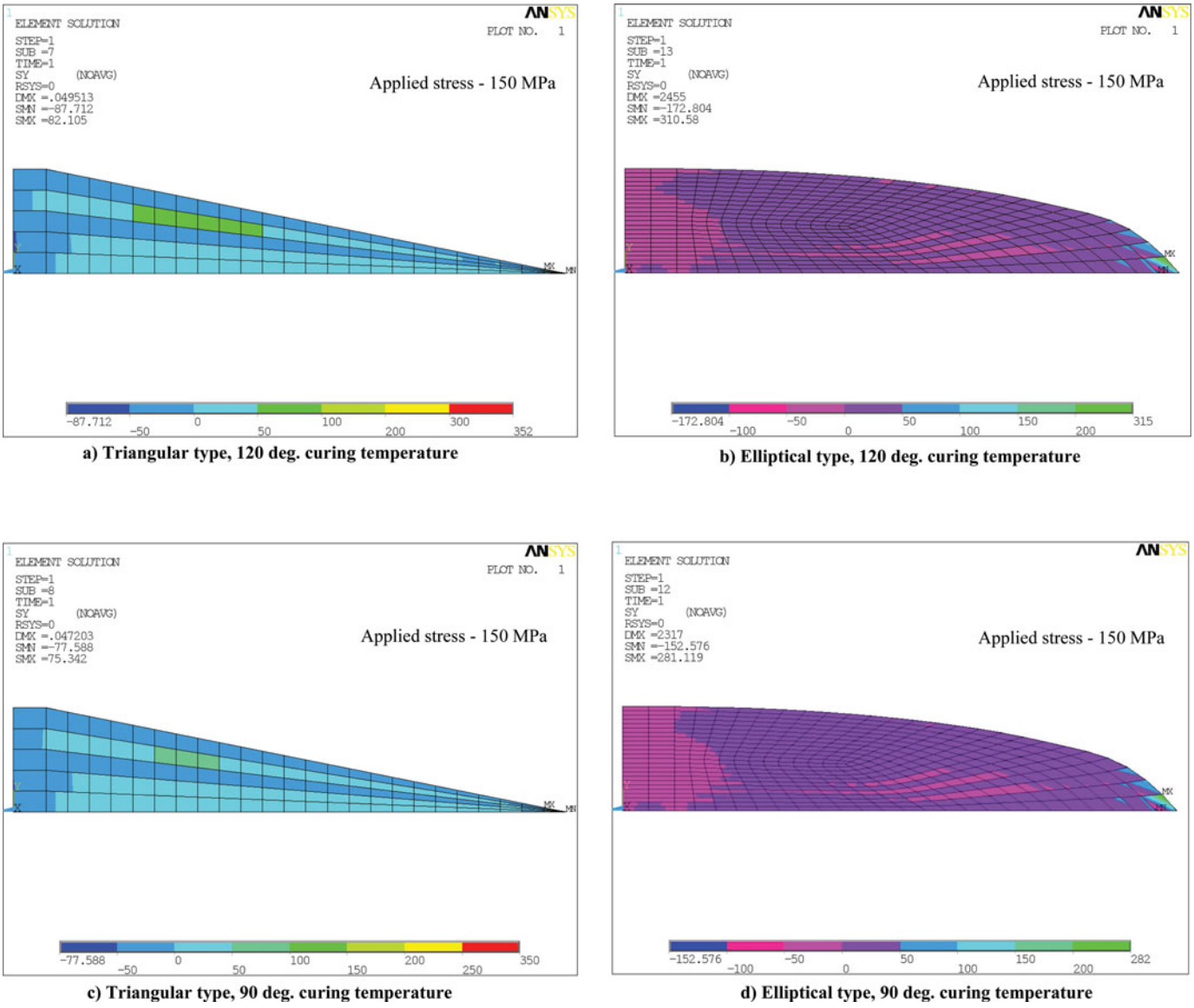

Fig. 12. Stress plots in y direction, $\sigma_{y,total,al}$, in delaminated aluminum zone of laminate with multiple delaminations.

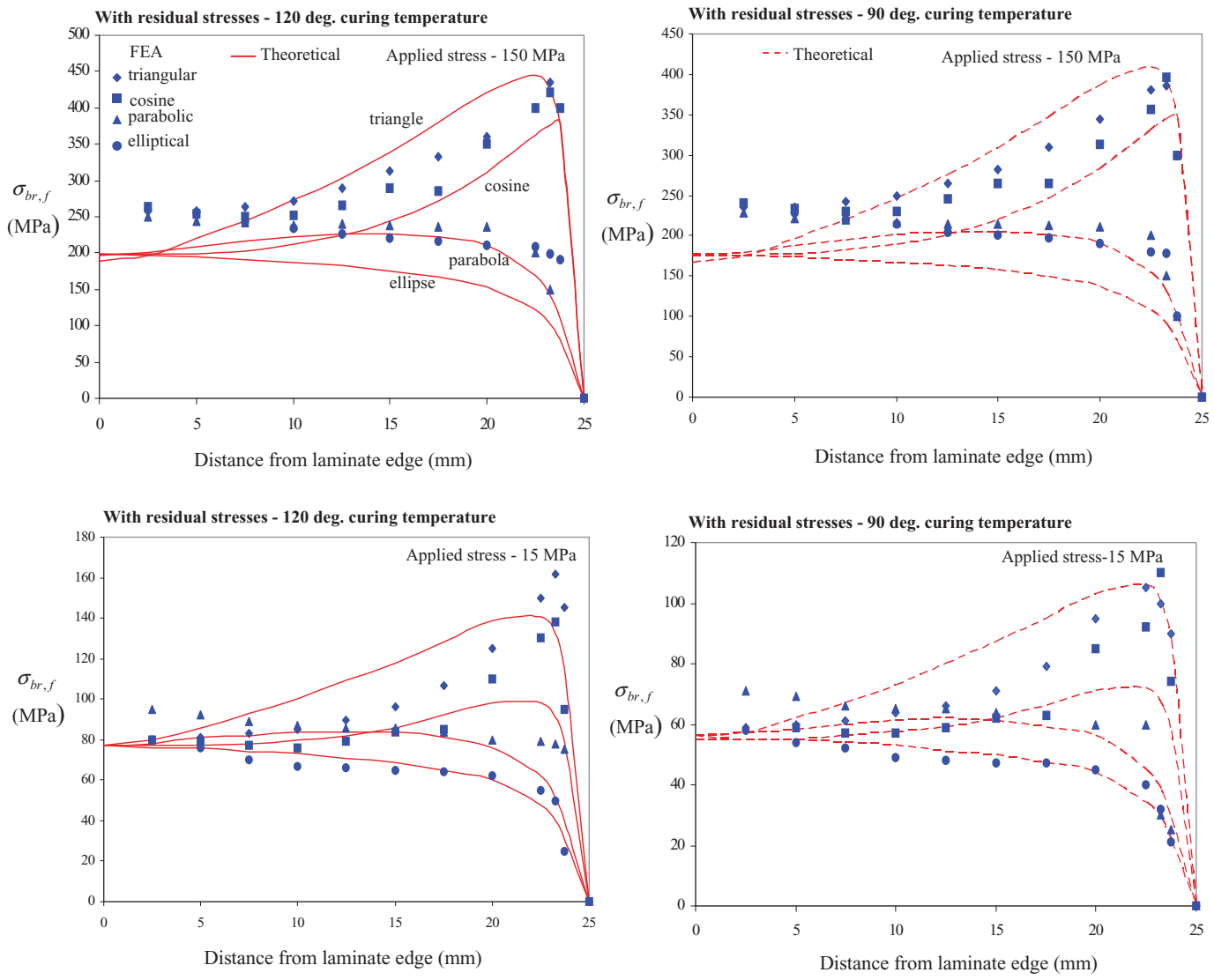

Fig. 13. Finite element values of fiber bridging stresses, $\sigma_{br,f}$, for different delamination shapes, in delaminated fiber zone of laminate with double delamination.

[27] is defined in x-y plane by Eq. (4):

$$J = \int_P \left(W_e dy - T_y \frac{\partial v_n}{\partial x} ds - T_x \frac{\partial u_n}{\partial x} ds \right), \qquad (4)$$

where $T_y = \sigma_y n_y + \tau_{xy} n_x$ and $T_x = \sigma_x n_x + \tau_{xy} n_y$. With n's in the expressions representing unit vectors in respective directions refer to Figure 8. J_{tip} is found over paths near the crack tip to numerically estimate the shielding effect due to fiber bridging at the crack tip.

4.1. *Results, Discussion, and Comparison with Theoretical Values*

Sample finite element plots of total load line or normal stress, $\sigma_{y,total,f}$, in the delaminated zone of a fiber layer in laminate, with double and multiple delaminations of triangular and elliptical types, under 150 MPa applied stress are illustrated in Figures 9 and 10. Similar plots for $\sigma_{y,total,al}$ in a delaminated aluminum zone are presented in Figures 11 and 12. Fulfillment of the conditions, $\sigma_{y,total,f} > \sigma_{y,induced,f}$ in fiber and $\sigma_{y,total,al} < \sigma_{y,induced,al}$ in aluminum substantiates load diversion to fiber with corresponding drop of stresses in aluminum in all of the cases. (Effect of bridging on an entire fiber layer is discussed in Section 4.2.) Plots with similar trends are obtained under 15 MPa stress also. $\sigma_{y,total,f}$ and $\sigma_{y,total,al}$ equal $(\sigma_{y,induced,f} + \sigma_{br,f})$ and $(\sigma_{y,induced,al} + \sigma_{br,al} + \sigma_{y,crack})$, respectively, where $\sigma_{y,crack}$ represents compressive stresses (-ve) due to the presence of a crack. The values of $\sigma_{br,f}$ along the crack depth are presented along with their theoretical values in Figures 13 and 14 for double and multiple delaminations of different shapes

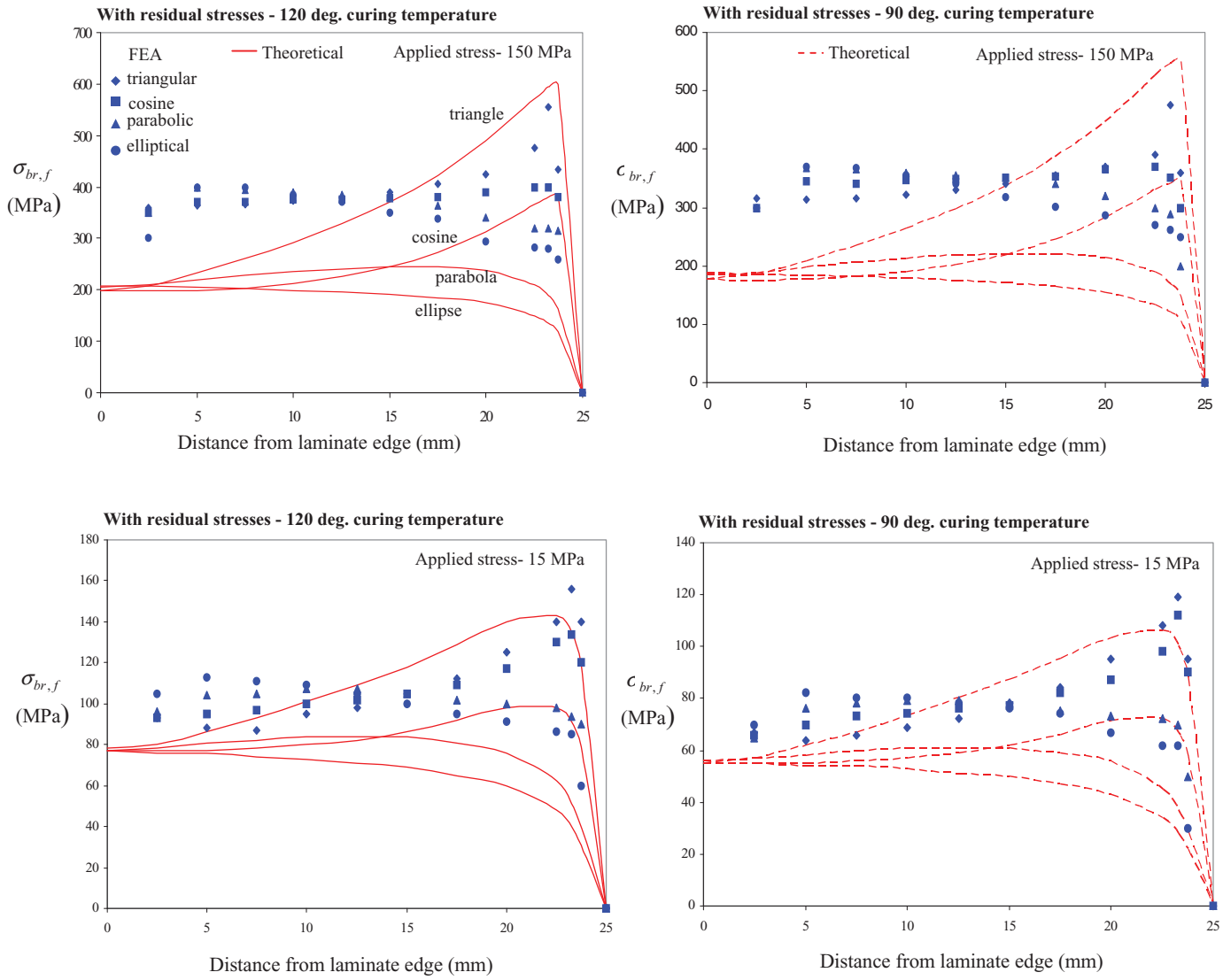

Fig. 14. Finite element values of fiber bridging stresses, $\sigma_{br,f}$, for different delamination shapes, in delaminated fiber zone of laminate with multiple delaminations.

respectively. The values are in good agreement with each other.

Referring to Figure 15, as expected the numerical size of load line stress lobe developed in aluminum (stress exceeding $\sigma_{y,induced,al}$) is minimum in triangular delamination and maximum in elliptical delamination due to maximum bridging in the former and minimum in the latter. J_{tip} values in all types of laminates are presented in Table 4. The size of normal crack tip plastic zone in the aluminum layer is found to be quite less than the crack length, which confirms small scale yielding regime. Therefore, the equation valid in LEFM for plane stress condition, $K_{tip} = \sqrt{E_{al} J_{tip}}$, is adopted to obtain K_{tip}. Like theoretical results, K_{tip} is least in the case of triangular delamination and maximum in the case of elliptical delamination, lower in the case of multiple delamination than in double delamination, and more in 120 deg. cured laminate than in 90 deg. cured type. However, the magnitude of K_{tip} is generally lower than its theoretical value in all the cases, the difference being minimum in triangular delamination and maximum in elliptical delamination. This is attributed to an upward shift in stresses away from the crack tip, the shift being minimum in triangular delamination and maximum in elliptical delamination. For instance, J integral path near the crack tip with elliptical delamination passes through the zone of low stresses thereby resulting in lower numerical values of J_{tip} and K_{tip} vis-à-vis the theoretical values, likewise in other delamination shapes too. Effect of the stress shift could not be captured in the theoretical model. Since the fiber bridging effect at normal crack tip is higher in multiple delamination than in double delamination, contrary to expectations that are

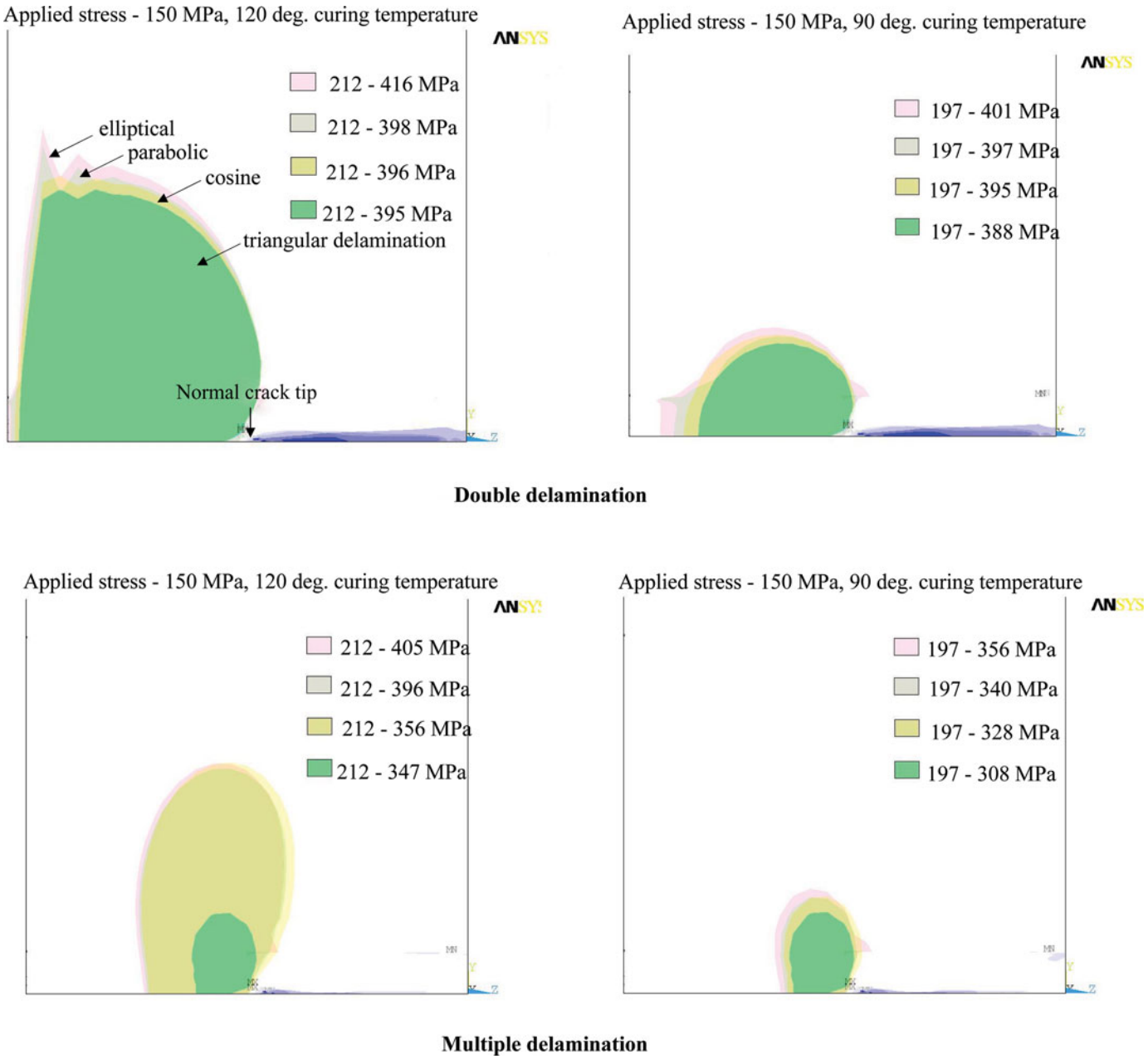

Fig. 15. Load line stress lobes in aluminum layer with different delaminations.

attributed to load transfer towards interfacial crack tips instead of normal crack tips during fiber bridging due to damage symmetry in multiple delamination case, the stress lobes are found to be smaller in the former than in the latter. Also, the stress lobes in both the cases are smaller at an applied stress of 15 MPa. ΔK_{tip} displays similar trends as those by the theoretical values.

Stresses exist along the thickness of the laminate (z direction) due to secondary bending effects. Sample lateral bending plots, deformations, and stress distribution in laminates with double and multiple delaminations of 120 deg. cured laminate with triangular delamination under applied stress of 150 MPa are illustrated in Figures 16 and 17.

4.2. *Influence of Delamination Growth Parameters on Fiber Bridging*

Laminate with multiple delaminations is considered for such an investigation because fiber bridging is higher in it than in the laminate with double delamination. Since the size of a delamination continuously changes with growth of normal and interfacial cracks and is therefore governed by the parameters

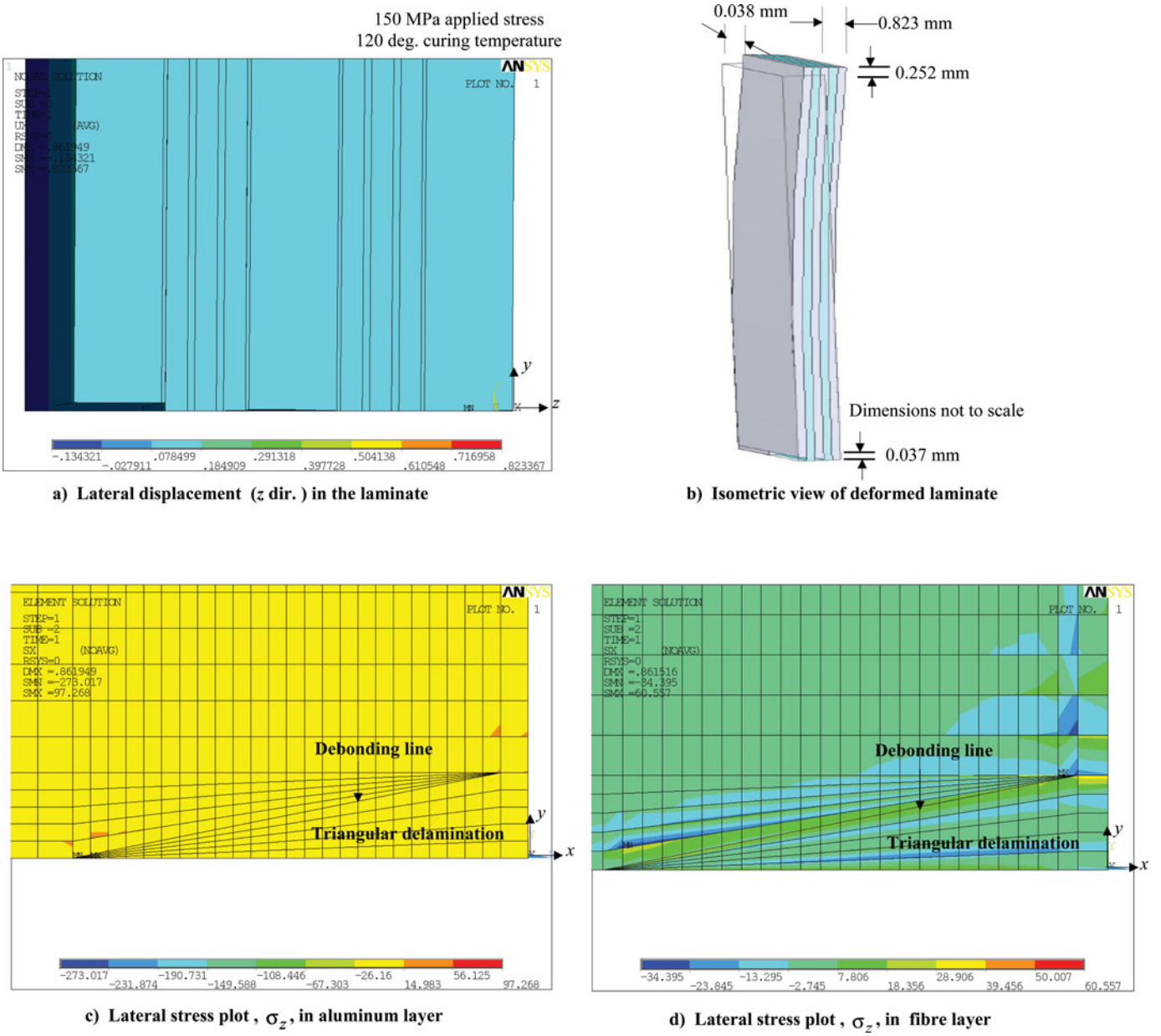

a) Lateral displacement (z dir.) in the laminate

b) Isometric view of deformed laminate

c) Lateral stress plot , σ_z, in aluminum layer

d) Lateral stress plot , σ_z, in fibre layer

Fig. 16. Secondary effects in laminate with double delamination.

c, b and the type of debonding curve, two sample discrete cases are examined in 120 deg. cured laminate with triangular debonding under monotonic load of 150 MPa, which are as follows: Case (a) Incremental normal crack growth without interfacial crack growth; Case (b) Incremental interfacial crack growth with unchanged normal crack length. Refer to Figure 18 for sample results in all fiber layers, f_1'' to f_6'', as shown in Figure 1. In each case, the total normal stress, $\sigma_{y,total^*,f}$, at all the nodes of a fiber layer are noted. The average stress value, $(\sigma_{y,total^*,f})_{av}$, of each fiber layer is found following which the average value of all six fiber layers, Π_f, equal to $\sum(\sigma_{y,total^*,f})_{av}/6$, is computed. The same process is undertaken for all three aluminum layers. Π_{al} is written as $\sum(\sigma_{y,total^*,al})_{av}/3$. In case (a) at fixed b of 4.7 mm and normal crack lengths of 24.9, 25, and 25.1 mm, the respective values of Π_f are 88.02, 88.09, and 88.46 MPa, and the respective values of Π_{al} are 200.35, 200.34, and 200.13 MPa. Likewise, the values in case (b) at fixed c of 25 mm and interfacial crack lengths of 4.6, 4.7, and 4.8 mm, the respective values of Π_f are 88.32, 88.09, and 87.85 MPa, and the respective values of Π_{al} are 200.22, 200.34, and 200.47 MPa. The results clearly demonstrate increase in fiber bridging with drop is stress state in aluminum layers as the normal crack grows and reduction in fiber bridging with increase in stress state in aluminum layers when the interfacial crack advances. Accordingly, K_{tip} and ΔK_{tip} values also fluctuate as the delamination size changes

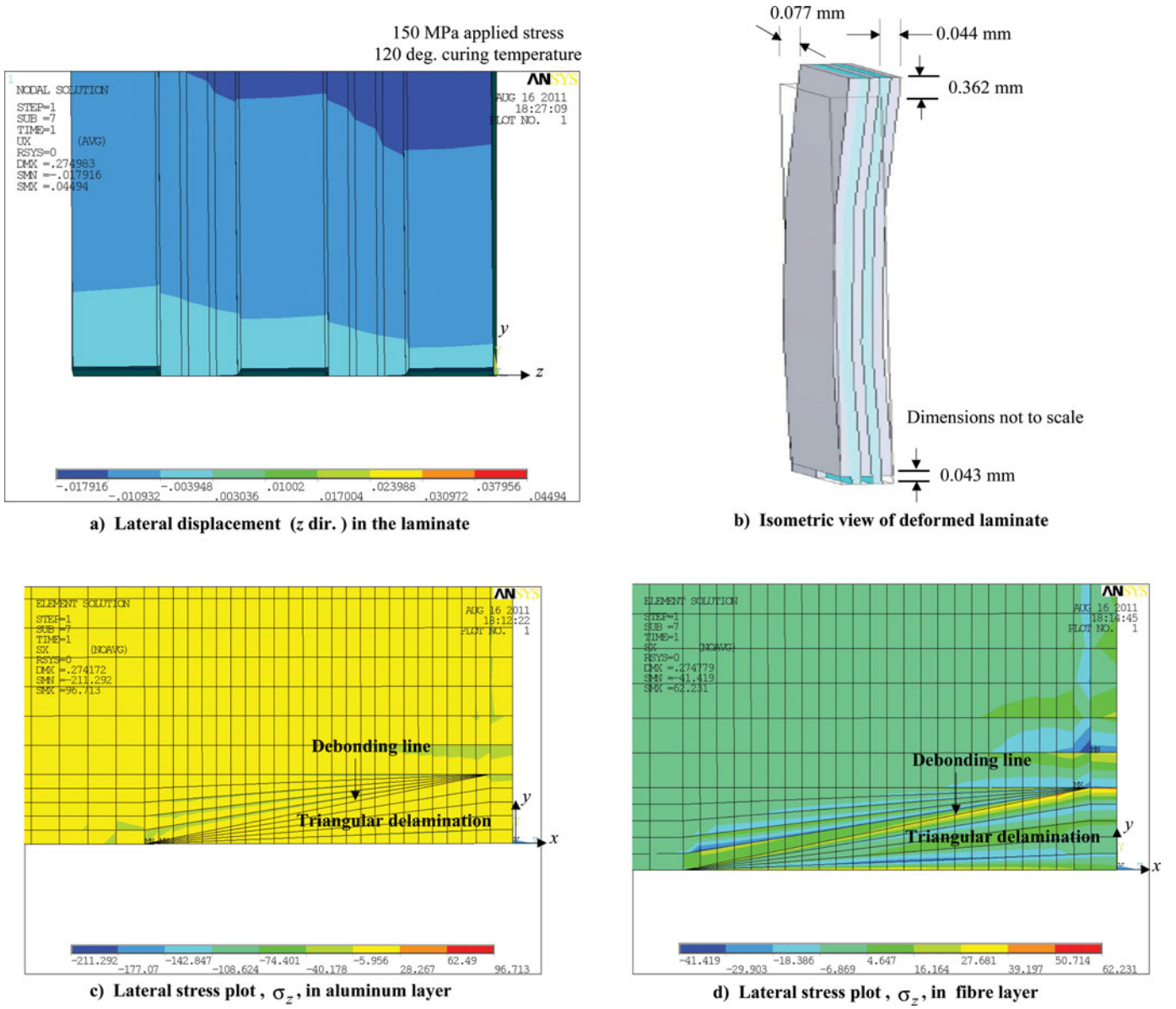

Fig. 17. Secondary effects in laminate with multiple delaminations.

longitudinally and laterally with increasing damage in the laminate. Load transfer effects are again convincingly proved since $\Pi_f > \sigma_{y,induced,f}$ and $\Pi_{al} < \sigma_{y,induced,al}$ in both the cases.

5. Conclusions

Residually stressed, cracked, and delaminated, Glare comprising three thin 2024-T3 aerospace aluminum alloy sheets alternatively bonded with two pre-pregs., each pre-preg. stacked with three epoxy resin impregnated E-glass fiber layers laid in 0, 90, and 0 deg. orientations, is theoretically and numerically investigated for fracture and fatigue characteristics. Laminates cured at temperatures of 90 deg. and 120 deg., subjected to constant monotonic tensile stress (150 MPa) and tension–tension (150 MPa–15 MPa) fatigue cycles, are considered for investigation. Double and multiple delaminations between aluminum and fiber layers, with triangular, cosine, parabolic, and elliptical debonding curves, are examined. A theoretical model is used to obtain stress intensity parameter at normal crack tip, K_{tip}, in aluminum layer under the influence of fiber bridging. Results of monotonic cases are extended to a cyclic regime.

Stress fields in delaminated zones of aluminum and fiber layers are obtained by finite element analysis. Fiber bridging resulting in load diversion to fibers with consequent shielding effect at normal crack tip is clearly noticed with all the types of delaminations. The effect is more in laminates with multiple delaminations than with double delamination. J_{tip} is found over the path near normal crack tip to determine K_{tip} numerically. Theoretical and numerical results support each other well and confirm the following:

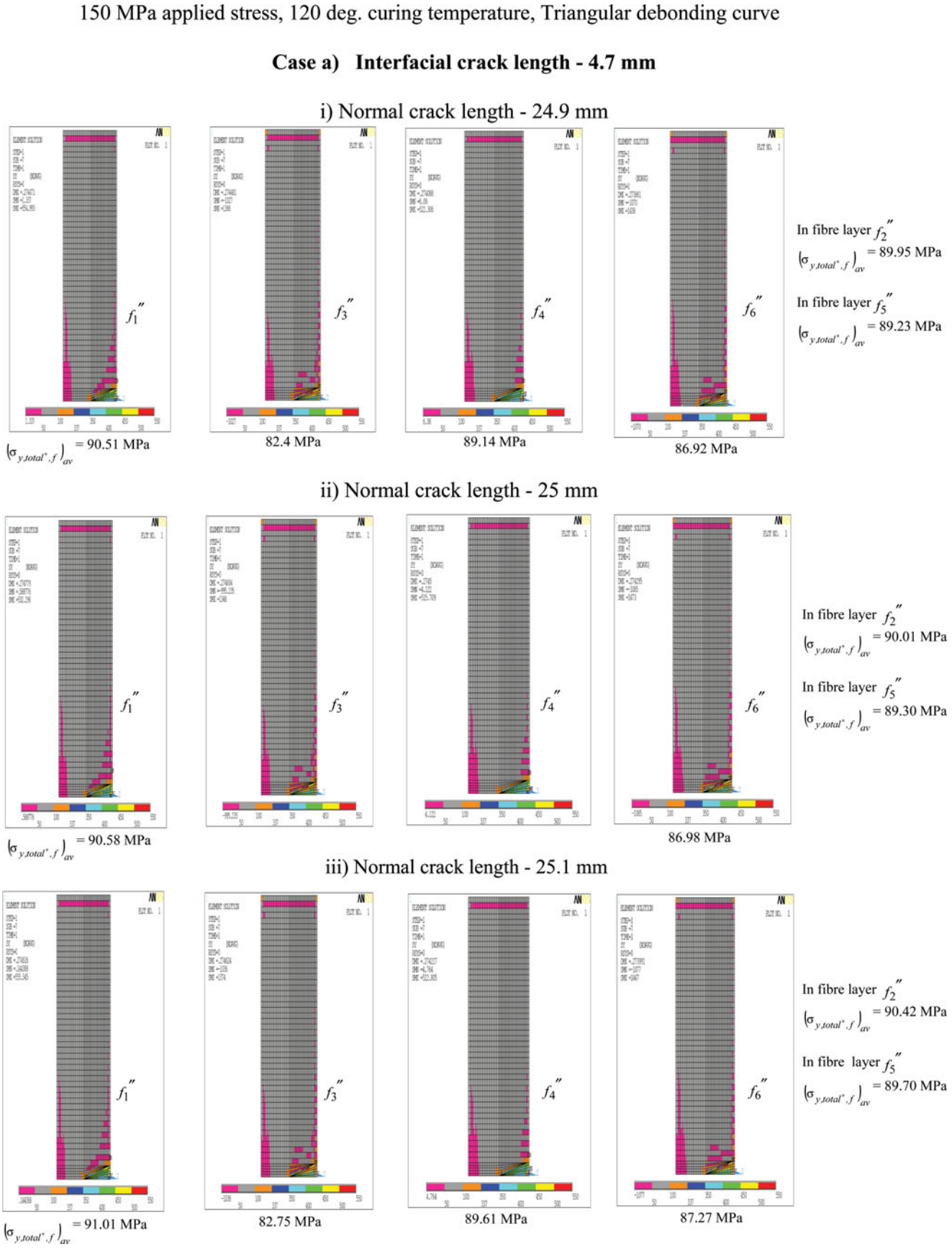

Fig. 18. Stress plots of entire fiber layers in y direction, $\sigma_{y,total^*,f}$, in laminate with multiple delaminations.

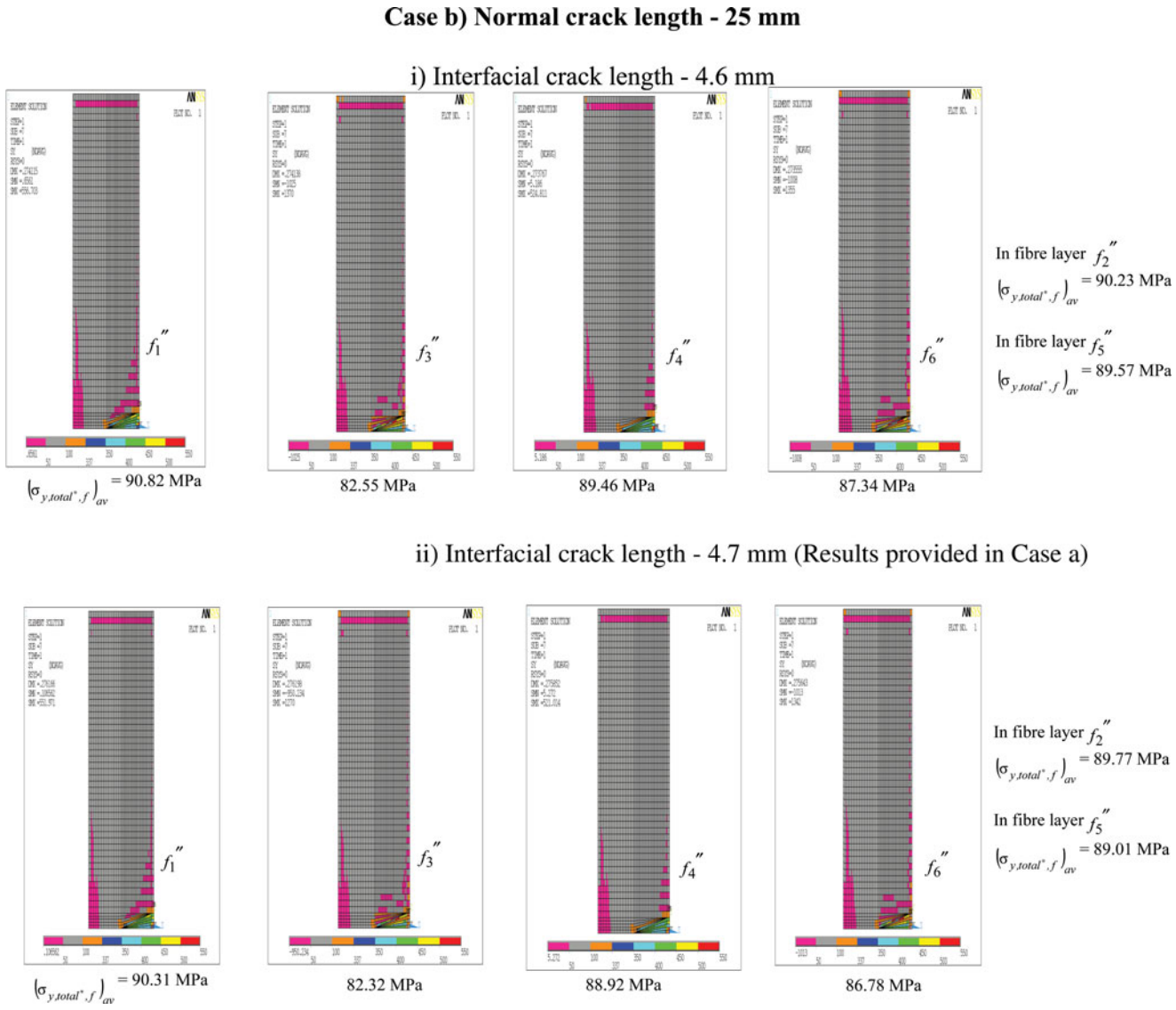

Fig. 18. (Continued)

(i) Fiber bridging is maximum in the laminate with triangular delamination and minimum in the laminate with elliptical delamination type, is more in 120 deg. cured laminate than in 90 deg. cured laminate, and is higher in laminate with multiple delaminations than with double delamination.

(ii) K_{tip} values are minimum in the case of triangular delamination and maximum in elliptical delamination, are less in laminate with multiple delamination than with double delamination. Although bridging is more in 120 deg. cured laminate than in 90 deg. cured laminate, K_{tip} is more in the former than in the latter.

(iii) With a particular delamination shape, ΔK_{tip} values are nearly the same in 90 deg. and 120 deg. cured laminates and are close to each other in laminates with double and multiple delaminations as well. As in monotonic load cases, ΔK_{tip} values are minimum in the case of triangular delamination and maximum in the case of elliptical delamination.

(iv) Delamination size parameters influence fiber bridging. Increase in delamination height by growth of interfacial crack reduces bridging and increases the stress state in the aluminum layer whereas an increase in delamination length by growth of a normal crack increases bridging and reduces the stress state in the aluminum layer.

Value of $K_{applied}$ for a thorough, Mode I, edge crack of 25 mm length in monolithic aluminum panel, of dimensions similar to Glare under investigation, is 118.86 MPa$\sqrt{\text{m}}$ when subjected to monotonic far field stress of 150 MPa. K_{tip} shall be equal to $K_{applied}$ since there is no shielding effect in homogenous aluminum. In comparison, theoretical K_{tip} values in Glare laminate are found to be much less, the maximum being 68.26 MPa$\sqrt{\text{m}}$ in 120 deg. cured laminate with elliptical delamination. Likewise, cyclic $\Delta K_{applied}$ or ΔK_{tip} values in aluminum panel under chosen load is 106.9 MPa$\sqrt{\text{m}}$. But maximum value of ΔK_{tip} is of the order of 55.5 MPa$\sqrt{\text{m}}$ in the laminate with elliptical delamination. Values from finite

element analysis are even less. A substantial drop in K_{tip} and ΔK_{tip} values in Glare, vis-a-vis monolithic aluminum panel, under all possible conditions, convincingly confirms improved fatigue and fracture properties of the laminate.

Acknowledgments

The authors wish to convey their thanks to Dr. S. Narayanan, Pro-Vice Chancellor of VIT, Vellore, India, for extending his kind support and cooperation during the execution of the project. Help received from other Senior authorities of VIT, Vellore is gratefully acknowledged.

Funding

The authors are grateful to the sanctioning authority of Science and Engineering Research Council (SERC), Department of Science and Technology (DST), India for funding the project.

References

[1] C.T. Lin, P.W. Kao, and F.S. Yang, Fatigue behaviour of carbon fibre-reinforced aluminum laminates, Composites, vol. 22, pp. 135–141, 1991.
[2] C.T. Lin and P.W. Kao, Effect of fibre bridging on the fatigue crack propagation in carbon fibre-reinforced aluminum laminates, Mat. Sci. Eng. A, vol. 190, pp. 65–73, 1995.
[3] C.T. Lin and P.W. Kao, Delamination growth and its effect on crack propagation in carbon fibre reinforced aluminum laminates under fatigue loading, Acta Mat., vol. 44, pp. 1181–1188, 1996.
[4] Y.J. Guo and X.R. Wu, A theoretical model for predicting fatigue crack growth rates in fibre-reinforced metal laminates, Fat. Frac. Eng. Mat. Str., vol. 21, pp. 1133–1145, 1998.
[5] Y.J. Guo and X.R. Wu, A phenomenological model for predicting crack growth in fibre reinforced metal laminates under constant amplitude loading, Com. Sci. Tech., vol. 59, pp. 1825–1831, 1999.
[6] Y.J. Guo and X.R. Wu, Bridging stress distribution in center-cracked fibre reinforced metal laminate: Modeling and experiment, Eng. Fra. Mech., vol. 63, pp. 147–163, 1999.
[7] K. Brown and A. Young, Fatigue crack growth in fibre reinforced metal laminates, Str. Mat., vol. 6, pp. 323–332, 2000.
[8] X.R. Wu and Y.J. Guo, Fatigue behaviour and life prediction of fibre reinforced metal laminates under constant and variable amplitude loading, Fat. Frac. Eng. Mat. Str., vol. 25, pp. 417–432, 2002.
[9] T. Takamatsu, T. Shimokawa, T. Matsumura, Y. Miyoshi, and Y. Tanabe, Evaluation of fatigue crack growth behaviour of GLARE 3 fibre/metal laminates using a compliance method, Eng. Fra. Mech., vol. 70, pp. 2603–2616, 2003.
[10] J.J. Homan, Fatigue initiation in fibre metal laminates, Int. J. Fat., vol. 28, pp. 366–374, 2006.
[11] R.C. Alderliesten and J.J. Homan, Fatigue and damage tolerance issues of Glare in aircraft structures, Int. J. Fat., vol. 28, pp. 1116–1123, 2006.
[12] A.S.J. Suiker and N.A. Fleck, Modelling of fatigue crack tunneling and delamination in layered composites, Composites, Part A: App. Sci. Mfg., vol. 37, pp. 1722–1733, 2006.
[13] R.C. Alderliesten, Analytical prediction model for fatigue crack propagation and delamination growth in Glare, Int. J. Fat., vol. 29, pp. 628–646, 2007.
[14] G. Wu, Y. Tan, and J.M.Yang, Evaluation of residual strength of notched fiber metal laminates, Mat. Sci. Eng. A, vol. 457, pp. 338–349, 2007.
[15] R.C. Alderliesten, G. Campoli, and R. Benedictus, Modelling cyclic shear deformation of fibre/epoxy layers in fibre metal laminates, Comp. Sci. Tech., vol. 67, pp. 2545–2555, 2007.
[16] H.M. Plokker, R.C. Alderliesten, and R. Benedictus, Crack closure in fibre metal laminates, Fat. Frac. Eng. Mat. Str., vol. 30, pp. 608–620, 2007.
[17] R.C. Alderliesten, On the available relevant approaches for fatigue crack propagation prediction in Glare, Int. J. Fat., vol. 29, pp. 289–304, 2007.
[18] P.Y. Chang and J.M. Yang, Modeling of fatigue crack growth in notched fibre metal laminates, Int. J. Fat., vol. 30, pp. 2165–2174, 2008.
[19] S.U. Khan, R.C. Alderliesten, and R. Benedictus, Post-stretching induced stress redistribution in fibre metal laminates for increased fatigue crack growth resistance, Comp. Sci. Tech., vol. 69, pp. 396–405, 2009.
[20] R.C Alderliesten and C. Rans, The meaning of threshold fatigue in fibre metal laminates, Int. J. Fat., vol. 31, pp. 213–222, 2009.
[21] S. Abdullah, A. Fahruddin, J. Syarif, M.Z. Omar, and R. Zulkifli, Fatigue crack growth modeling of fibre metal laminate (FML) composite, Eur. J. Sci. Res., vol. 35, pp. 43–53, 2009.
[22] R. Rodi, R.C. Alderliesten, and R. Benedictus, Experimental characterization of the crack-tip-opening angle in fibre metal laminates, Eng. Fra. Mech., vol. 77, pp. 1012–1024, 2010.
[23] W.D. Callister Jr., Materials Science and Engineering: An Introduction, 6th Edition, John Wiley and Sons, Inc., New Delhi, India, 2004, pp. 737–754.
[24] A. Vlot and J.W. Gunnink, Fibre Metal Laminates—An Introduction, Kluwer Academic Publisher, The Netherlands, 2001, p. 5.
[25] K. Hellan, Introduction to Fracture Mechanics, McGraw-Hill Book Company, New York, NY, 1985, p. 244.
[26] J.M. Gere, Mechanics of Materials, 6th Edition, Thomson Learning, London, U.K., 2004, pp. 146–147.
[27] J.R. Rice, A path independent integral and approximate analysis of strain concentration by notches and cracks, J. App. Mech., vol. 35, pp. 379–386, 1968.

Appendix A

Fundamental Equations

$$v_f = \frac{V_f}{V_f + V_r}, \tag{A1}$$

$$v_r = \frac{V_r}{V_f + V_r} = 1 - v_f, \tag{A2}$$

$$v'_{al} = \frac{3V_{al}}{4V_{c0} + 2V_{c90} + 3V_{al}}, \tag{A3}$$

$$v'_{c0} = \frac{4V_{c0}}{4V_{c0} + 2V_{c90} + 3V_{al}}, \tag{A4}$$

$$v'_{c90} = \frac{2V_{c90}}{4V_{c0} + 2V_{c90} + 3V_{al}}, \tag{A5}$$

$$E_{lc} = E_f v_f + E_r v_r, \tag{A6}$$

$$E_{tc} = \frac{E_f E_r}{v_f E_r + v_r E_f}, \tag{A7}$$

$$\mu_{c0} = \mu_{c90} = \mu_{xy} = \mu_{yz} = \frac{\mu_f \mu_r}{v_f \mu_r + v_r \mu_f}, \tag{A8}$$

$$E_{ll} = E_{lc} v'_{c0} + E_{al} v'_{al} + E_{tc} v'_{c90}, \tag{A9}$$

$$E_{tl} = \frac{1}{\frac{v'_{al}}{E_{al}} + \frac{v'_{c90}}{E_{tc}} + \frac{v'_{c0}}{E_{lc}}}, \tag{A10}$$

$$\nu_{majc} = \nu_f v_f + \nu_r v_r, \tag{A11}$$

$$\nu_{\min c} = \nu_{majc} \frac{E_{tc}}{E_{lc}}, \tag{A12}$$

$$\nu_{majl} = \nu_{majc} v'_{c0} + \nu_{al} v'_{al} + \nu_{minc} v'_{c90}, \tag{A13}$$

$$\alpha_{lc} = \frac{E_f \alpha_f v_f + E_r \alpha_r v_r}{E_f v_f + E_r v_r}, \tag{A14}$$

$$\alpha_{tc} = \alpha_f v_f (1 + \nu_f) + \alpha_r v_r (1 + \nu_r) - \nu_{majc} \alpha_{lc}, \tag{A15}$$

$$\alpha_{ll} = \frac{E_{lc} \alpha_{lc} v'_{c0} + E_{tc} \alpha_{tc} v'_{c90} + E_{al} \alpha_{al} v'_{al}}{E_{lc} v'_{co} + E_{tc} v'_{c90} + E_{al} v'_{al}}, \tag{A16}$$

$$\alpha_{tl} = \alpha_{lc} v'_{c0} (1 + \nu_{majc}) + \alpha_{al} v'_{al} (1 + \nu_{al}) + \alpha_{tc} v'_{c90} (1 + \nu_{minc}) - \nu_{majl} \alpha_{ll}. \tag{A17}$$

Appendix B

Constitutive Equations (Plane Stress)

(A) Aluminum and Pre-preg.

(i) Aluminum:

$$\sigma_x = \frac{E_{al}}{1 - \nu_{al}^2} \{\varepsilon_x + \nu_{al} \varepsilon_y\}$$
$$\sigma_y = \frac{E_{al}}{1 - \nu_{al}^2} \{\nu_{al} \varepsilon_x + \varepsilon_y\};$$
$$\tau_{xy} = \mu_{al} \gamma_{xy}$$

Stiffness matrix,

$$\{\mathrm{M}\}_{al} = \begin{bmatrix} \frac{E_{al}}{1 - \nu_{al}^2} & \frac{E_{al}}{1 - \nu_{al}^2} \nu_{al} & 0 \\ \frac{E_{al}}{1 - \nu_{al}^2} \nu_{al} & \frac{E_{al}}{1 - \nu_{al}^2} & \\ 0 & 0 & \mu_{al} \end{bmatrix}.$$

(ii) Composite, $c0$:

$$\sigma_x = \frac{E_{tc}}{(1 - \nu_{majc} \nu_{minc})} \{\varepsilon_x + \nu_{majc} \varepsilon_y\}$$
$$\sigma_y = \frac{E_{lc}}{(1 - \nu_{majc} \nu_{minc})} \{\nu_{minc} \varepsilon_x + \varepsilon_y\};$$
$$\tau_{xy} = \mu_{c0} \gamma_{xy}$$

Stiffness matrix, $\{\mathrm{M}\}_{c0}$

$$= \begin{bmatrix} \frac{E_{tc}}{(1 - \nu_{majc} \nu_{minc})} & \frac{E_{tc}}{(1 - \nu_{majc} \nu_{minc})} \nu_{majc} & 0 \\ \frac{E_{lc}}{(1 - \nu_{majc} \nu_{minc})} \nu_{minc} & \frac{E_{lc}}{(1 - \nu_{majc} \nu_{minc})} & 0 \\ 0 & 0 & \mu_{c0} \end{bmatrix}.$$

(iii) Composite, $c90$:

$$\sigma_x = \frac{E_{lc}}{(1 - \nu_{majc} \nu_{minc})} \{\varepsilon_x + \nu_{\min c} \varepsilon_y\}$$
$$\sigma_y = \frac{E_{tc}}{(1 - \nu_{majc} \nu_{minc})} \{\nu_{majc} \varepsilon_x + \varepsilon_y\};$$
$$\tau_{xy} = \mu_{c90} \gamma_{xy}$$

Stiffness matrix, $\{\mathrm{M}\}_{c90}$

$$= \begin{bmatrix} \frac{E_{lc}}{(1 - \nu_{majc} \nu_{minc})} & \frac{E_{lc}}{(1 - \nu_{majc} \nu_{minc})} \nu_{minc} & 0 \\ \frac{E_{tc}}{(1 - \nu_{majc} \nu_{minc})} \nu_{majc} & \frac{E_{tc}}{(1 - \nu_{majc} \nu_{minc})} & 0 \\ 0 & 0 & \mu_{c90} \end{bmatrix};$$

Stiffness matrix of laminate,

$$\{\mathrm{M}\}_{lam} = \{\mathrm{M}\}_{al} \times \frac{0.4 \times 3}{2.0} + \{\mathrm{M}\}_{c0} \times \frac{0.133 \times 4}{2.0} + \{\mathrm{M}\}_{c90} \frac{0.133 \times 2}{2.0};$$

Applied stress over laminate,

$$\sigma_{applied} = \begin{Bmatrix} \sigma_x \\ \sigma_y \\ \tau_{xy} \end{Bmatrix}_{applied};$$

Strain in laminate,

$$\varepsilon_{lam} = \begin{Bmatrix} \varepsilon_x \\ \varepsilon_y \\ \gamma_{xy} \end{Bmatrix}_{lam} = \{\mathrm{M}\}_{lam}^{-1} \sigma_{applied};$$

Induced stress in each laminate layer,

$$\sigma_{induced} = \begin{Bmatrix} \sigma_x \\ \sigma_y \\ \tau_{xy} \end{Bmatrix}_{induced};$$

Without residual stresses:
In aluminum, $\{\sigma\}_{induced,al} = \{\mathrm{M}\}_{al} \times \varepsilon_{lam}$;
In composite $c0$, $\{\sigma\}_{induced,c0} = \{\mathrm{M}\}_{c0} \times \varepsilon_{lam}$;
In composite $c90$, $\{\sigma\}_{induced,c90} = \{\mathrm{M}\}_{c90} \times \varepsilon_{lam}$.
With residual stresses:
Residual strain:

$$\text{Aluminum, } \{\varepsilon\}_{al,rs} = \left[\begin{Bmatrix} \alpha_x \\ \alpha_y \\ 0 \end{Bmatrix}_{al} - \begin{Bmatrix} \alpha_{tl} \\ \alpha_{ll} \\ 0 \end{Bmatrix} \right] \times \left(T'_{curing} - T'_{ambient}\right);$$

$$\text{Composite c0, } \{\varepsilon\}_{c0,rs} = \left[\begin{Bmatrix}\alpha_{tc}\\ \alpha_{lc}\\ 0\end{Bmatrix} - \begin{Bmatrix}\alpha_{tl}\\ \alpha_{ll}\\ 0\end{Bmatrix}\right] \times \left(T'_{curing} - T'_{ambient}\right);$$

$$\text{Composite c90, } \{\varepsilon\}_{c90,rs} = \left[\begin{Bmatrix}\alpha_{lc}\\ \alpha_{tc}\\ 0\end{Bmatrix} - \begin{Bmatrix}\alpha_{tl}\\ \alpha_{ll}\\ 0\end{Bmatrix}\right] \times \left(T'_{curing} - T'_{ambient}\right);$$

$$\{\sigma\}_{induced,al} = \{M\}_{al} \times \left[\varepsilon_{lam} + \{\varepsilon\}_{al,rs}\right];$$

$$\{\sigma\}_{induced,c0} = \{M\}_{c0} \times \left[\varepsilon_{lam} + \{\varepsilon\}_{c0,rs}\right];$$

$$\{\sigma\}_{induced,c90} = \{M\}_{c90} \times \left[\varepsilon_{lam} + \{\varepsilon\}_{c90,rs}\right].$$

(B) Individual Layers

(i) Aluminum:

$$\sigma_x = \frac{E_{al}}{\left(1-\nu_{al}^2\right)}\left\{\varepsilon_x + \nu_{al}\varepsilon_y\right\}$$
$$\sigma_y = \frac{E_{al}}{\left(1-\nu_{al}^2\right)}\left\{\nu_{al}\varepsilon_x + \varepsilon_y\right\}.$$
$$\tau_{xy} = \mu_{al}\gamma_{xy}$$

(ii) Resin:

$$\sigma_x = \frac{E_r}{\left(1-\nu_r^2\right)}\left\{\varepsilon_x + \nu_r\varepsilon_y\right\}$$
$$\sigma_y = \frac{E_r}{\left(1-\nu_r^2\right)}\left\{\nu_r\varepsilon_x + \varepsilon_y\right\}.$$
$$\tau_{xy} = \mu_r\gamma_{xy}$$

(iii) Fiber:

$$\sigma_x = \frac{E_f}{\left(1-\nu_f^2\right)}\left\{\varepsilon_x + \nu_f\varepsilon_y\right\}$$
$$\sigma_y = \frac{E_f}{\left(1-\nu_f^2\right)}\left\{\nu_f\varepsilon_x + \varepsilon_y\right\}.$$
$$\tau_{xy} = \mu_f\gamma_{xy}$$

$\{M\}_{al}$, $\{M\}_f$, and $\{M\}_r$ are obtained in a similar manner as discussed earlier.

Stiffness matrix of laminate:

$$\{M\}_{lam} = \{M\}_{al} \times \frac{0.4\times 3}{2.0} + \{M\}_f \times \frac{0.1\times 6}{2.0} + \{M\}_r \times \frac{0.0165\times 12}{2.0};$$

Residual strain:

$$\text{Aluminum, } \{\varepsilon\}_{al,rs} = \left[\begin{Bmatrix}\alpha_x\\ \alpha_y\\ 0\end{Bmatrix}_{al} - \begin{Bmatrix}\alpha_{tl}\\ \alpha_{ll}\\ 0\end{Bmatrix}\right] \times \left(T'_{curing} - T'_{ambient}\right);$$

$$\text{Resin, } \{\varepsilon\}_{r,rs} = \left[\begin{Bmatrix}\alpha_x\\ \alpha_y\\ 0\end{Bmatrix}_{r} - \begin{Bmatrix}\alpha_{tl}\\ \alpha_{ll}\\ 0\end{Bmatrix}\right] \times \left(T'_{curing} - T'_{ambient}\right);$$

$$\text{Fibre, } \{\varepsilon\}_{f,rs} = \left[\begin{Bmatrix}\alpha_x\\ \alpha_y\\ 0\end{Bmatrix}_{f} - \begin{Bmatrix}\alpha_{tl}\\ \alpha_{ll}\\ 0\end{Bmatrix}\right] \times \left(T'_{curing} - T'_{ambient}\right).$$

Induced stresses, with and without residual stresses, are found in a similar manner as discussed in Part A.

Appendix C

The equation of deformation at $x = x_i$ in the delamination zone is written as:

$$\delta_c(x_i) + \delta_{ad}(x_i) = u^*_{induced}(x_i) - u^*_{br}(x_i) + \delta_{al}, \tag{C1}$$

$$\delta_c(x_i) = \left(\frac{2\left[\sigma_{y,induced,c0} + \sigma_{br,f}(x_i)\right]}{E_{lc}} + \frac{\left[\sigma_{y,induced,c90} + \sigma_{br,f}(x_i)\right]}{E_{tc}}\right) b_i, \tag{C2}$$

$$\delta_{ad}(x_i) = (N_b)_i \sigma_{y,induced,al} t_{al} \frac{t_{c0}}{\mu_{c0}} \sqrt{\left(n_1\frac{\mu_{c0}}{t_{c0}} + n_2\frac{\mu_{c90}}{t_{c90}}\right) \times \left(\frac{1}{n_3 t_{al} E_{al}} + \frac{1}{n_1 E_{lc} t_{c0} + n_2 E_{tc} t_{c90}}\right)}, \tag{C3}$$

where $(N_b)_i = 1 - [\cosh\sqrt{\alpha_{ud}}b_i - \tanh\sqrt{\alpha_{ud}}b_i \sinh\sqrt{\alpha_{ud}}b_i]$, $b_i = b.f(c, c', x_i)$ and

$$\alpha_{ud} = 2\left[\frac{n_1\frac{1}{t_{c0}E_{lc}} + n_2\frac{1}{t_{c90}E_{tc}}}{n_1\frac{t_{c0}}{\mu_{c0}} + n_2\frac{t_{c90}}{\mu_{c90}}}\right].$$

$$u^*_{induced}(x_i) = \frac{2\sigma_{y,induced,al}}{E_{al}}\sqrt{c^2 - x_i^2}, \tag{C4}$$

$$u^*_{br}(x_i) = \int_0^c u^*\left(x_i, x_j\right) dx_j, \tag{C5}$$

where displacement at a point due to bridging is given as follows:

$$u^*\left(x_i, x_j\right) = \frac{4}{\pi E_{ll}}\left(\tanh^{-1}\sqrt{\frac{c^2 - x_j^2}{c^2 - x_i^2 + b_j^2}} + \frac{\frac{1}{2}(1+\nu_{majl})b_j^2}{x_j^2 - x_i^2 + b_j^2} \times \sqrt{\frac{c^2 - x_j^2}{c^2 - x_i^2 + b_j^2}}\right)\sigma_{br,f}(x_j). \quad \text{(C6)}$$

(If $x_i > x_j$, replace x_i by x_j and x_j by x_i.)

δ_{al} is the deformation in aluminum layer which is negligible and is not considered. Bridging stresses (compressive, -ve) in aluminum are given by:

$$\sigma_{br,al}(x_j) = -\sigma_{br,f}(x_j)\frac{n_1 t_{c0} + n_2 t_{c90}}{n_3 t_{al}}. \quad \text{(C7)}$$

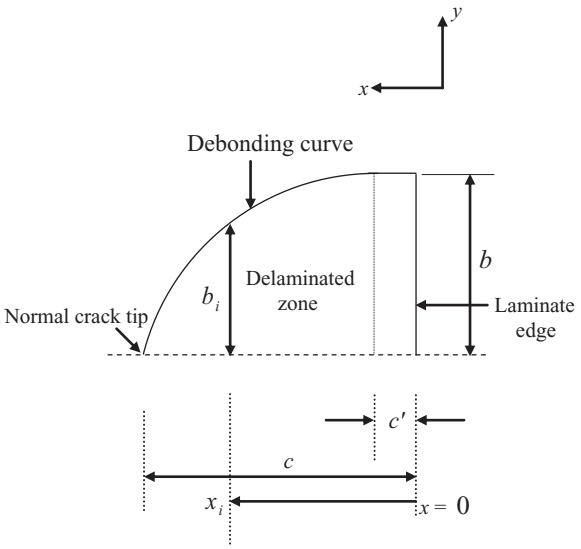

$b_i = b\frac{c-x_i}{c-c'}$ (Triangular delamination); $b_i = b\sqrt{\frac{c-x_i}{c-c'}}$ (Parabolic delamination) $b_i = b\sqrt{1-\left(\frac{x_i-c'}{c-c'}\right)^2}$ (Elliptical delamination); $b_i = b\cos\left[\frac{\pi}{2}\left(\frac{x_i-c}{c-c'}\right)\right]$ (Cosine delamination)